



HAL
open science

Assessment of numerical schemes for complex two-phase flows with real equations of state

Philippe Helluy, Olivier Hurisse, Lucie Quibel

► **To cite this version:**

Philippe Helluy, Olivier Hurisse, Lucie Quibel. Assessment of numerical schemes for complex two-phase flows with real equations of state. *Computers and Fluids*, 2020, 196 (104347). hal-02315038v1

HAL Id: hal-02315038

<https://hal.science/hal-02315038v1>

Submitted on 14 Oct 2019 (v1), last revised 17 Jun 2020 (v2)

HAL is a multi-disciplinary open access archive for the deposit and dissemination of scientific research documents, whether they are published or not. The documents may come from teaching and research institutions in France or abroad, or from public or private research centers.

L'archive ouverte pluridisciplinaire **HAL**, est destinée au dépôt et à la diffusion de documents scientifiques de niveau recherche, publiés ou non, émanant des établissements d'enseignement et de recherche français ou étrangers, des laboratoires publics ou privés.

Assessment of numerical schemes for complex two-phase flows with real equations of state.

Philippe Helluy[†]
helluy@unistra.fr

Olivier Hurisse^{*}
olivier.hurisse@edf.fr

Lucie Quibel[◇]
lucie.quibel@edf.fr

^{†,◇} *IRMA, UMR CNRS 7501, 7 rue Descartes, 67000 Strasbourg, France.*

^{*,◇} *EDF R&D, 6 quai Watier, 78400 Chatou, France.*

Key words : Two-phase flow, mass transfer, Look-up table, Nucleation.

Abstract

Some accidental scenarii studied in the framework of the nuclear safety analysis involve liquids undergoing strong pressure drops at high temperature. In order to perform realistic simulations of such situations, a code based on a model that can handle both the thermodynamical disequilibrium between liquid and vapor and complex equations of state is required. We propose herein to test a homogeneous model built on the basis of the Euler system of equations and complemented by a mixture pressure law. The latter is defined in accordance with the Gibbs relation on the basis of the phasic pressures which are defined through a look-up table based on the IAPWS-97 formulation. A wide range of verification problems (Riemann problems) is then studied to assess the behavior of the numerical schemes for this complex equation of state. The tested relaxation scheme is the best compromise between accuracy and stability. At last, a simple test case of vaporization near a wall is investigated in order to test some return to thermodynamical-equilibrium time-scale based on the nucleation theory.

Introduction

A nuclear pressurized water reactor (PWR) is composed of several heat exchangers in which the water is used as a heat-transfer medium and can undergo phase change (vaporization and condensation). A PWR contains two main loops in which water flows in liquid or vapour state: the primary and the secondary circuits, exchanging heat through the steam generator. The primary circuit contains liquid water which collects the heating power of the nuclear core and brings it into the steam-generator. In this circuit, the temperature can reach 320°C and, to avoid vaporization, the pressure is maintained at 155 bars, that means, above the saturation pressure. In the steam generator, the primary coolant flows into pipes that are surrounded by the water of the secondary circuit. The secondary fluid enters the steam generator as liquid. It then receives heat of the primary coolant on contact with the primary pipes and vaporizes. The steam-generator's outlet of the secondary circuit is then mainly composed of steam. The latter is used to generate electric power through turbines and it is afterwards condensed (through the use of an other heat-exchanger and a third circuit) to re-enter the steam generator as liquid. In this secondary circuit, the pressure level is much lower than in the primary circuit (in the range 50 – 70 bars, depending on the steam generator).

When the reactor is at nominal operating point, the mass transfer and the heat exchanges imply small thermodynamical variations. Nevertheless, when accidental scenarii are considered, brutal thermodynamical variations are assumed. For instance, if one focuses on the breaches in the shell of the primary circuit, two major scenarii are studied.

- The Loss Of Coolant Accident (or LOCA) corresponds to a breach for which the primary liquid coolant enters into contact with the air of the reactor building at 1 bar. The violent pressure drop from 155 bars to 1 bar implies a rapid blowdown and the propagation of a depressurization wave into the primary circuit. This depressurization is associated with the vaporization of the primary coolant.
- When a breach in a pipe that contains the primary coolant in the steam generator occurs, the pressurized liquid water enters into contact with a steam-liquid mixture at a lower pressure. As in the LOCA situation, a depressurization wave propagates into the primary circuit leading to the steam creation in the primary loop.

These two scenarii are associated with high pressure drops and high temperatures. In such situations, the fast transients can thus lead to non-equilibrium thermodynamics [1]. Hence, the simulation of such rapid transients requires a model in which the thermodynamical disequilibria between the two phases are taken into account.

A first class of models that can be used for such scenarii is the so-called two-fluid model as those proposed in [2, 3, 4, 5, 6, 7]. In this class of models, the full thermodynamical disequilibrium is accounted for, in terms of the pressure, the temperature and the chemical potential (or Gibbs free enthalpy). Moreover, each phase is described by its own velocity.

This two-velocity assumption has a drawback when dealing with the numerical simulation. Indeed, these models can possess eigenvalues that are very close to each other, for instance in situations involving a strong drag force. In order to distinguish the different waves associated with these close eigenvalues on the numerical approximations, one can thus have to deal with meshes that contain small enough cells, leading to an unaffordable computational cost for industrial applications in 3D. In the sequel, we choose to present a model that possesses a simpler eigenstructure. The latter makes the assumption that the two phases have the same velocity and is based on a model relying on the Euler set of equations. Therefore, the model inherits the Euler eigenstructure and enters the so-called class of the homogeneous models.

Most of two-phase flow homogeneous models proposed since around 40 years are based on one or more thermodynamical equilibrium assumptions (for instance: [3, 8, 9, 10, 11, 12, 13]). The homogeneous model used in this work does not make any equilibrium assumption for the thermodynamics: the phasic temperatures, pressures and chemical potentials may be different within each phase. On the one hand, this choice has been made to account for the full thermodynamical disequilibrium: the pressure disequilibrium may allow to enrich the model by introducing a bubble dynamics model as proposed in [7, 14, 15]. On the other hand, this allows to tackle some specificity of the mixture Equations Of States (EOS) obtained with equilibrium assumptions. It has indeed been reported that equilibrium assumptions may lead to a loss of strict concavity of the mixture entropy [16, 17, 18] and then to non-uniqueness of solutions of the Riemann problems.

This homogeneous model proposed in [16, 19, 20], and studied for instance in [9, 21, 22, 23], is based on the Euler system of equations complemented by a complex pressure law and by three unknowns: a **volume** fraction, a **mass** fraction and an **energy** fraction. These fractions allow to quantify the gap to the equilibrium state, reached when the system is isolated from the surroundings. In the model, the return to this equilibrium state is ensured by three source terms on the fractions involving a **unique** relaxation time-scale law. The whole model is built in order to be consistent with the second law of thermodynamics and is hyperbolic if each phasic entropy is concave with respect to the phasic specific volume and the phasic specific internal energy, and if the mixture temperature is positive [18, 24, 25]. The model and its properties are presented in section 1.

The model has been tested either on Riemann problems [24, 26] and on simulations reproducing elementary experimental facilities [25]. In both cases, the phasic EOS were defined through Stiffened Gas EOS [27] which is an extension of the perfect gas EOS. Even if the results presented in [25] are satisfactory, the Stiffened Gas EOS is too rough to describe **accurately** all the thermodynamical properties of the water on situations with **large variations** of the thermodynamical states, such as those depicted above. A look-up table has then been developed, based on the idea of [28] and using the IAPWS-97 [29] formulation as input data. The main recipes of this look-up table are presented in section 2.

The whole numerical scheme is described in section 3. In [24, 25, 26], the numerical schemes used to compute the numerical approximations of the solutions of the model were all robust enough to deal with Stiffened Gas EOS. Unfortunately, few of these numerical schemes are able to handle complex EOS as the one proposed in section 2. Indeed, three numerical schemes for the convective part have been tested : the Rusanov scheme [30], a VFRoe-ncv scheme [31] and a relaxation scheme [32], based on the ideas of [33, 34, 35, 36]. In practise, problems of robustness have been encountered with VFRoe-ncv scheme used with the look-up table; therefore, only Rusanov scheme and the relaxation scheme have been compared when using it. In section 4, their behavior is then studied on a wide range of Riemann problems for the EOS defined through the look-up table of section 2. This verification procedure is mandatory to grasp the behavior of the numerical schemes in canonical situations. Furthermore it is required in the framework of the safety studies, where proofs of confidence on the simulation tools are to be given. The relaxation scheme is the best compromise between accuracy and robustness when using the look-up table.

In [25], the impact of the relaxation time-scale law has been shown by the mean of toy laws. These laws have no physical background, and they are based on the observations reported in [12]. In section 5, we propose a model for the relaxation time-scale on the basis of the classical nucleation theory [37], with some simple assumptions used in [38] or [39]. Since the nucleation theory only holds for the birth of steam bubbles in liquid, we have chosen a situation where the domain is entirely filled with liquid and where steam production remains reasonable: a depressurization occurring near a wall. This case can be schematic of what happens downstream a valve suddenly closed in a pipe in which high pressurized water flows. One can note that a very similar phenomenon occurs in the early stage of the SUPERCANON experiment reported in [40] and which was reproduced in [25].

1 A homogeneous model for two-phase flows

In this section, the considered model is only briefly presented in intensive variables. The whole building approach is available in appendix A, starting from an extensive description of the system by a volume \mathcal{V} (in m^3) of the mixture, corresponding to a mass \mathcal{M} (in kg) and an internal energy \mathcal{E} (in J).

Thermodynamically, each phase $k = l, v$ (liquid or vapor) is described by its own complete equation of state, expressed as a specific entropy $s_k(\tau_k, e_k)$ ($JK^{-1}kg^{-1}$) as a function of τ_k the specific volume (m^3kg^{-1}) and e_k the specific energy (Jkg^{-1}) and satisfying the Gibbs relation:

$$T_k ds_k = de_k + P_k d\tau_k, \quad (1)$$

where

$$\frac{1}{T_k} = \left. \frac{\partial s_k}{\partial e_k} \right|_{\tau_k} ; \quad \frac{P_k}{T_k} = \left. \frac{\partial s_k}{\partial \tau_k} \right|_{e_k}. \quad (2)$$

Let us introduce the volume fraction α_k , the mass fraction y_k and the energy fraction z_k of phase k :

$$Y_k = (\alpha_k, y_k, z_k). \quad (3)$$

These fractions satisfy conservation relations:

$$1 = \alpha_l + \alpha_v ; \quad 1 = y_l + y_v ; \quad 1 = z_l + z_v, \quad (4)$$

and vary in accordance with the second principle of thermodynamics (cf appendix A). Thanks to them, phasic quantities can be expressed from the mixture quantities:

$$\tau_k = \frac{\alpha_k}{y_k} \tau ; \quad e_k = \frac{z_k}{y_k} e. \quad (5)$$

The mixture entropy s is defined as:

$$s(Y, \tau, e) = y_l s_l(\tau_l, e_l) + y_v s_v(\tau_v, e_v). \quad (6)$$

Using phasic Gibbs relations (1), thermodynamical mixture quantities can be deduced from phasic ones; they read:

$$P(Y, \tau, e) = \frac{\alpha_l \frac{P_l}{T_l} + \alpha_v \frac{P_v}{T_v}}{\frac{z_l}{T_l} + \frac{z_v}{T_v}} ; \quad \frac{1}{T}(Y, \tau, e) = \frac{z_l}{T_l} + \frac{z_v}{T_v}. \quad (7)$$

The set of partial differential equations in conservative form is:

$$\begin{cases} \frac{\partial}{\partial t} (\rho Y) + \frac{\partial}{\partial x} (\rho U Y) = \rho \Gamma, \\ \frac{\partial}{\partial t} (\rho) + \frac{\partial}{\partial x} (\rho U) = 0, \\ \frac{\partial}{\partial t} (\rho U) + \frac{\partial}{\partial x} (\rho U^2 + P) = 0, \\ \frac{\partial}{\partial t} (\rho E) + \frac{\partial}{\partial x} (U(\rho E + P)) = 0. \end{cases} \quad (8)$$

with the following source terms:

$$\Gamma = \left(\frac{\bar{\alpha}_l - \alpha_l}{\lambda}, \frac{\bar{y}_l - y_l}{\lambda}, \frac{\bar{z}_l - z_l}{\lambda} \right),$$

where $(\bar{\alpha}_l, \bar{y}_l, \bar{z}_l)$ are the equilibrium fractions which maximize the mixture entropy for a given (τ, e) . The user must specify one EOS (see section 2) for each phase and the time-scale $\lambda > 0$ describing the return to the thermodynamical equilibrium (see section 5 and appendix C).

It can be shown that this model has interesting mathematical properties. These properties are summarized here and the reader can refer to [16, 18, 19, 20, 21, 22, 25, 41] for more details.

- The eigenstructure of the model is composed of 2 genuinely non-linear waves associated to the eigenvalues $U \pm c$, where c is the mixture sound speed, and one linearly degenerate wave associated to the eigenvalue U .
- The model is hyperbolic provided that the phasic entropies s_k are concave (see (H_7) in appendix A) and that the mixture temperature is non-negative. The condition on the mixture temperature is of importance. Indeed, the concavity of the entropies together with the positivity of the mass fractions guarantees that c^2/T is non-negative. However some simple EOS (as the Van der Waals EOS) admit non-positive energy. This may lead to non-positive energy fractions and a possible drawback is to get a negative mixture temperature even when assumption (H_9) (see appendix A) holds. Such situations can then correspond to a loss of hyperbolicity.
- Shocks are defined in a unique manner through the Rankine-Hugoniot relations.
- Assuming classical assumptions on the initial and boundary conditions for the fractions, and provided that the equilibrium fractions remain in $[0, 1]^3$, the fractions remain in $[0, 1]^3$.

2 Complex equations of state

In order to close the model presented in section 1, we need to specify: one EOS for each phase in terms of the specific entropy $(\tau_k, e_k) \mapsto s_k(\tau_k, e_k)$, and a law for the time-scale λ which describes the return to the thermodynamical equilibrium defined by \bar{W} . We focus here on the phasic EOS.

A classical way to deal with steam-liquid simulation is to use Stiffened Gas EOS [27]. These EOS are extensions of the perfect gas EOS. They are associated with quite simple formula involving five parameters. The specific phasic entropy then reads:

$$s_k(\tau_k, e_k) = C_{v,k} \ln \left((e_k - \Pi_k \tau_k) \tau_k^{\gamma_k - 1} \right) + s_k^0, \quad (9)$$

where $C_{v,k}$ is the heat capacity, $-\Pi_k$ is the minimal pressure¹, γ_k is the adiabatic coefficient ($\gamma_k > 1$) and s_k^0 is a reference specific-entropy.

In the situations that we intend to address, the domain of evolution of the thermodynamical quantities is important and these Stiffened Gas EOS may be not accurate enough, at least not for all the quantities. A more complex EOS with a better description of the properties of the fluids on wide domains is thus needed. Such EOS have been proposed, as Cubic EOS or Viriel formulations, but they are unfortunately not in complete form [18], which means that some thermodynamical quantities may not be defined. The IAPWS-97 formulation [29] is defined in a complete form since the the EOS is given as the Gibbs free enthalpy with respect to the pressure and the temperature. Nevertheless, this function is very complex and an important drawback is the high computational cost which is a crucial point for the simulation of fluid dynamics. In order to decrease this computational cost, a **Look-up Table** (LuT) has been implemented on the basis of the IAPWS-97 formulation².

We describe here how this LuT is built. Since the model deals with non-equilibrium thermodynamics and since each phase has to possess its own EOS, a LuT is built for each phase.

The (P, T) -plane is chosen as an entry of the LuT and the Gibbs free enthalpy $\mu_k(P, T)$ is given for each phase. In order to remain consistent with the Gibbs relation for each phase (1), all the other quantities have to be computed from the derivatives of

$$\mu_k(P, T) = e_k(P, T) + P\tau_k(P, T) - Ts_k(P, T).$$

Indeed, by differentiating μ_k and by using the phasic Gibbs relation (1) we get:

$$d\mu_k = \tau_k dP - s_k dT,$$

¹The phasic entropy and the phasic sound speeds are defined for $P_k > -\Pi_k$; and the phasic temperature is positive for $P_k > -\Pi_k$

²The methodology proposed here to build a LuT is obviously not restricted to the IAPWS formulation.

so that the specific volume and the specific entropy are respectively defined as:

$$\tau_k(P, T) = \partial\mu_k/\partial P|_T \quad \text{and} \quad s_k(P, T) = -\partial\mu_k/\partial T|_P.$$

The specific energy then follows $e_k(P, T) = \mu_k(P, T) - P\tau_k(P, T) + Ts_k(P, T)$.

Remark 1. *In order to fulfill the phasic Gibbs relation (1), the quantities τ_k , s_k and e_k should not be tabulated independently.*

As in [28], the thermodynamical plane (P, T) is discretized using a Quadtree approach which is balanced to get a regular discretization of the plane, enabling a quick research through the look-up table in practical simulations. Some domains of the (P, T) -plane are refined. This is actually the case: in the neighborhood of the saturation curve, at low pressures, at low temperatures and at high pressures on the saturation curve. The LuT used in the next sections has been built for pressures from 0.1 bar to 219 bars, so that we avoid vicinity of the critical point. The temperature range is [283.0 K; 1070.0 K].

Figure 1 shows some visualizations of the quadtree mesh for different ranges of pressures and temperatures. On each cell of the (P, T) -plane, the IAPWS-97 Gibbs enthalpy μ_k is interpolated using a polynomial spline in P and T . The most important point is to preserve the Gibbs relations (1). It is required that μ_k belongs to \mathcal{C}^1 on the whole domain. Therefore, splines of order 3 are used and a specific treatment is applied to each cell connected to wider cells. For these cells, at each node that is common with a wider cell, the values of μ_k and its derivatives are not obtained from IAPWS-97. These values are replaced by the values of μ_k and its derivatives computed from the interpolated spline of the wider cell. Hence we ensure the continuity of the interpolated value μ_k and of its derivatives with respect to P and T at the junction between the cells of different sizes. For this purpose, the computation of the spline coefficients is then done by decreasing order of the size of the cells. The final level of refinement of the quadtree is chosen so as to get a relative error between the IAPWS values of μ_k and the interpolated values less than a threshold. In the LuT used in the next sections, this threshold has been chosen equal to 10^{-5} , and the final mesh contains more than 163000 cells.

The use of meshes based on quadtree techniques is a great advantage because it allows the local refinement of the description together with a reasonable computational cost for the search of the cell in which the properties have to be estimated. In fact, for a given (P^0, T^0) , the cost of the search of the quadtree's cell containing (P^0, T^0) is proportional to the depth of this cell in the quadtree structure (i.e. the smaller the target cell is, the more expensive its search is).

We are dealing with compressible phenomena so that the model of section 1 has to be discretized in conservative form (numerical schemes are described in section 3). Hence the “natural” variables for the conservative part of the model are (τ, e) . Since the LuT EOS is defined in the (P, T) -plane, and in order to maintain the consistency of the thermodynamical description through a complete LuT, we need to compute the change of variables

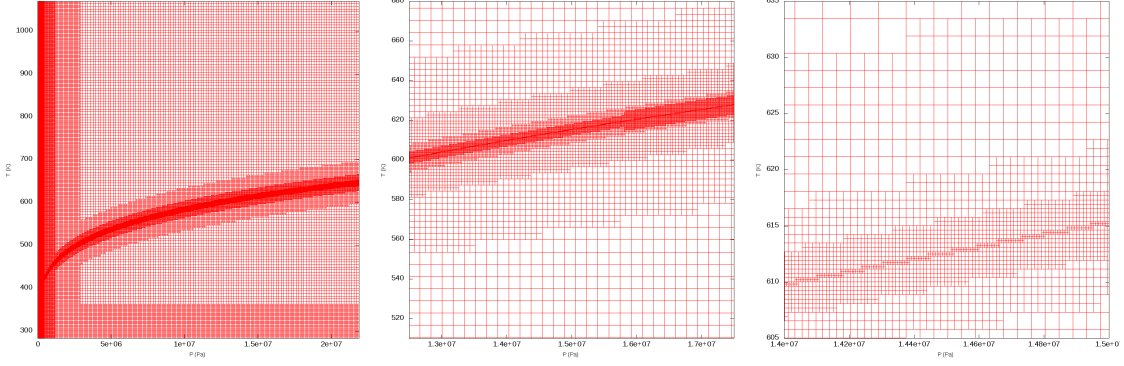


Figure 1: Mesh of the (P, T) -plane. The left figure shows the whole mesh, and the log-like domain corresponds to the mesh refinement around the saturation curve. The two figures on the right show zooms on the saturation curve zone.

$(\tau_k, e_k) \mapsto (P_k, T_k)$. More precisely, for any value of the specific volume τ_k^0 and specific energy e_k^0 , we have to find the pressure P_k and the temperature T_k that fulfill:

$$\begin{cases} e_k(P_k, T_k) = e_k^0, \\ \tau_k(P_k, T_k) = \tau_k^0, \end{cases} \quad (10)$$

where the functions $(P_k, T_k) \mapsto e_k(P_k, T_k)$ and $(P_k, T_k) \mapsto \tau_k(P_k, T_k)$ are obtained from the LuT. From a numerical point of view, the computation of an approximate solution of (10) through a Newton-type algorithm can be tricky and it requires an accurate initial guess of the solution. For this purpose, a second LuT has been built for each phase. This second LuT is based on a non-balanced quadtree for the (τ, e) -plane. At each vertex (τ_k^i, e_k^i) of the mesh corresponds a couple (P_k^i, T_k^i) such that $e_k(P_k^i, T_k^i) = e_k^i$ and $\tau_k(P_k^i, T_k^i) = \tau_k^i$. This second LuT is not used directly, but using bilinear interpolation, it represents a database to provide initial guesses to solve the general problem (10). With the help of this second LuT, solving (10) requires less iterations and it is more robust. For the sections below, this second LuT contains 166000 cells.

Remark 2. *In practice, considering the Stiffened Gas EOS as a reference, the order of magnitude of the computation costs is 700 times higher for the direct IAPWS formulation and it is 8 times higher with the LuT EOS as depicted above. Obviously, the gain in CPU time strongly depends on the test case and on the LuT used (the local refinement and the depth of the quadtree are strongly involved).*

3 Numerical method

The overall numerical method is based on a fractional step method [42] using a Lie-Trotter splitting. The initial condition problem associated with system of equations (8) can be written:

$$\frac{\partial}{\partial t} (W) = -\frac{\partial}{\partial x} (\mathcal{F}(W)) + \mathcal{G}(W), \quad W(t=0) = W^0, \quad (11)$$

where \mathcal{F} correspond to the convective flux and \mathcal{G} to the source terms. A straightforward Lie-Trotter splitting has been chosen here. It consists in solving at time $t = t^n$ the following two sub-systems during a time step Δt^n :

$$(i) \quad \frac{\partial}{\partial t} (W_a) = -\frac{\partial}{\partial x} (\mathcal{F}(W_a)), \quad W_a(t^n) = W^n, \quad (12)$$

which gives $W_a(t^n + \Delta t^n)$;

$$(ii) \quad \frac{\partial}{\partial t} (W_b) = \mathcal{G}(W_b), \quad W_b(t = t^n) = W_a(t^n + \Delta t^n). \quad (13)$$

Since this splitting is first order with respect to time, each sub-system is solved using first order schemes.

The first sub-system takes into account the convective part. For that purpose, first-order explicit and conservative finite volumes schemes are used. Their general form for a one-dimensional framework with cells Ω_i is:

$$|\Omega_i|(W_i^{n+1} - W_i^n) = -\Delta t^n ((F(W_i^n, W_{i+1}^n) - F(W_{i-1}^n, W_i^n)), \quad (14)$$

where W_i^n denotes the space-average value of W on the cell Ω_i at time t^n . The time step Δt^n is computed from the variable W_i^n and from the mesh size $|\Omega_i|$ in order to fulfill stability constraint. The two-point numerical flux F depends on the used scheme. In the following, we have tested three different schemes: Rusanov scheme [30], a VFRoe-ncv scheme using variables (Y, τ, U, P) [31] and the relaxation scheme proposed in [32]. These schemes are described in section 3.1.

The second sub-system (13) corresponds to a system of ordinary derivative equations. In this sub-system, the return to equilibrium is accounted for. Since the time-step is computed to fulfill a stability constraint of the numerical scheme used for the first sub-system, this second step is achieved using an implicit scheme. The latter is detailed in section 3.2.

Remark 3. *For the sake of simplicity, each sub-system is solved using a unique time-step and the time-step for solving the source-terms step is the time-step computed for the convective part.*

3.1 Numerical schemes for the convective sub-system

This section is devoted to the numerical schemes used to compute the two-point numerical fluxes F considering two neighboring cells. The quantities in the cell on the left (resp. right) of the interface between the two cells are denoted by a subscript l (resp. r).

Rusanov scheme (see [30]) and VFRoe-ncv scheme using variables (u, P, τ) (see [31]) are very classical and the details about these schemes can be found in the previous references.

The studied relaxation scheme was initially proposed in [32] and it is based on the work of [33, 34, 35, 43]. The main idea is to compute the numerical flux on the basis of an enlarged hyperbolic system associated with a strong relaxation term. This enlarged system is chosen so that all its characteristic fields are linearly degenerate. Hence, the solution of the associated Riemann problem at each interface between two cells is easy to compute. The relaxation term, accounted for in the enlarged system by a source term, then allows to recover formally the initial system of equations.

We follow here the proposition detailed in [32]. One additional scalar unknown \mathcal{T} is introduced with the initial condition:

$$\forall x, \mathcal{T}(0, x) = \tau(0, x).$$

A new pressure Π is also defined, which can be seen as a linearization of the pressure P with respect to the variable τ around \mathcal{T} :

$$\Pi = P(Y, \mathcal{T}, e) + a^2(\mathcal{T} - \tau), \quad (15)$$

where a is a positive parameter. At last, a relaxation specific total energy Σ is introduced in order to be consistent with the pressure Π :

$$\Sigma = \frac{u^2}{2} + e + \frac{\Pi^2 - P^2(Y, \mathcal{T}, e)}{2a^2}, \quad (16)$$

We set Z the enlarged variable: $Z = (Y, \tau, U, \Sigma, \mathcal{T})$. The enlarged system to solve is then the following:

$$\begin{cases} \partial_t(\rho Y) + \partial_x(\rho Y U) = 0 \\ \partial_t \rho + \partial_x(\rho U) = 0 \\ \partial_t(\rho U) + \partial_x(\rho U^2 + \Pi) = 0 \\ \partial_t(\rho \Sigma) + \partial_x(\rho U \Sigma + U \Pi) = 0 \\ \partial_t(\rho \mathcal{T}) + \partial_x(\rho \mathcal{T} U) = \frac{1}{\epsilon} \rho(\tau - \mathcal{T}) \end{cases} \quad (17)$$

where the relaxation source terms for \mathcal{T} is characterized by the parameter $\epsilon \geq 0$. A crucial point is that all the characteristic fields of the convective part of system (17) are linearly degenerate and associated with the speed waves:

$$\lambda_1 = U_l - a\tau_l, \quad \lambda_2 = U^*, \quad \lambda_3 = U_r + a\tau_r, \quad (18)$$

with:

$$U^* = \frac{1}{2}(U_l + U_r) + \frac{1}{2a}(\Pi_l - \Pi_r). \quad (19)$$

The parameter a , that appears in the definitions of Π and σ (resp. (15) and (16)), should satisfy a stability condition [35] which is related to the sub-characteristic condition for the enlarged system (17):

$$a > \max\left(\frac{c_l(Y_l, \tau_l, e_l)}{\tau_l}, \frac{c_r(Y_r, \tau_r, e_r)}{\tau_r}\right), \quad (20)$$

where $c(Y, \tau, e)$ denotes the sound speed associated with the pressure law P :

$$c(Y, \tau, e) = -\tau^2 \left. \frac{\partial}{\partial \tau} (P) \right|_{Y,s}.$$

Moreover, a is chosen so that the eigenvalues fulfill the relation:

$$\lambda_1 < \lambda_2 < \lambda_3, \quad (21)$$

where λ_k is detailed in (18); this last condition is equivalent to:

$$\tau_l^* > 0 \quad \text{and} \quad \tau_r^* > 0. \quad (22)$$

Thanks to relations (21), the self-similar solution $\mathcal{Z}(x/t, Z_l, Z_r)$ of the Riemann problem at the interface separating two cells (l and r) for the convective part of system (17) can be written:

$$\mathcal{Z}\left(\frac{x}{t}, Z_l, Z_r\right) = \begin{cases} Z_l, & \text{if } x/t < \lambda_1 \\ Z_l^*, & \text{if } \lambda_1 < x/t < \lambda_2 \\ Z_r^*, & \text{if } \lambda_2 < x/t < \lambda_3 \\ Z_r, & \text{if } \lambda_3 < x/t \end{cases} \quad (23)$$

with

$$\tau_l^* = \tau_l + \frac{1}{a}(U^* - U_l) \quad ; \quad \tau_r^* = \tau_r - \frac{1}{a}(U^* - U_r) \quad ; \quad (24)$$

$$\Sigma_l^* = \Sigma_l + \frac{1}{a}(\Pi_l U_l - \Pi^* U^*); \Sigma_r^* = \Sigma_r - \frac{1}{a}(\Pi_r U_r - \Pi^* U^*) \quad ; \quad (25)$$

$$\mathcal{T}_l^* = \mathcal{T}_l \quad ; \quad \mathcal{T}_r^* = \mathcal{T}_r \quad ; \quad Y_l^* = Y_l; \quad Y_r^* = Y_r \quad ; \quad (26)$$

$$U_l^* = U_r^* = U^* \quad ; \quad \Pi_l^* = \Pi_r^* = \Pi^* \quad (27)$$

where we have set:

$$\Pi^* = \frac{1}{2}(\Pi_l + \Pi_r) + \frac{a}{2}(U_l - U_r)$$

and where U^* is given in (19). From a numerical point of view, we have chosen an instantaneous relaxation: $\epsilon \rightarrow 0$. As a consequence, we have $\mathcal{T} \rightarrow \tau$, $\Pi \rightarrow P$ and $\Sigma \rightarrow E$, so that the two-point numerical flux corresponding to the relaxation scheme [32] is solely

based on the value $\mathcal{Z}(x/t = 0, Z_l, Z_r)$ of the solution \mathcal{Z} at the interface between the two-cells l and r . It reads:

$$F(W_l, W_r) = \left(\frac{YU}{\tau}, \frac{U}{\tau}, \frac{U^2}{\tau} + \Pi, \frac{U\Sigma}{\tau} + U\Pi \right),$$

where Y , τ , U , and Σ are the components of $\mathcal{Z}(x/t = 0, Z_l, Z_r)$ and where Π also arises from the solution $\mathcal{Z}(x/t = 0, Z_l, Z_r)$.

Remark 4. *For all the simulations that we have performed, the choice of λ in agreement with the constraint (20) has always been sufficient to ensure that the constraint (21) was fulfilled.*

We briefly recall some important properties of the relaxation scheme, proved in [44] for a more general context of Euler system with several pressures. In the following, index j refers to one mesh cell:

- \mathcal{L}_1 stability: $\rho_j^{n+1} > 0$ and $e_j^{n+1} > 0 \forall j$;
- discrete entropy inequality:

$$\rho S_j^{n+1} \leq \rho S_j^n - \frac{\Delta t}{\Delta x} \{(\rho S u)(0; Z_j^n; Z_{j+1}^n) - (\rho S u)(0; Z_{j-1}^n; Z_j^n)\};$$

- maximum principle:

$$\min(S_{j-1}^n, S_j^n, S_{j+1}^n) \leq S_j^{n+1} \leq \max(S_{j-1}^n, S_j^n, S_{j+1}^n).$$

3.2 Numerical scheme for the source-term sub-system

The second sub-system (13) corresponds to a system of ordinary differential equations:

$$\left\{ \begin{array}{l} \frac{\partial}{\partial t} (Y) = \frac{\bar{Y}(\tau, e) - Y}{\lambda} \\ \frac{\partial}{\partial t} (\rho) = 0 \\ \frac{\partial}{\partial t} (\rho U) = 0 \\ \frac{\partial}{\partial t} (\rho E) = 0. \end{array} \right. \quad (28)$$

We first remark that the specific volume and the specific energy are constant, as a consequence it can be written in an equivalent manner:

$$\left\{ \begin{array}{l} \frac{\partial}{\partial t} (Y(t)) = \frac{\bar{Y}(\tau(0), e(0)) - Y(t)}{\lambda(t)} \\ \frac{\partial}{\partial t} (\rho(t)) = 0 \\ \frac{\partial}{\partial t} (U(t)) = 0 \\ \frac{\partial}{\partial t} (e(t)) = 0. \end{array} \right. \quad (29)$$

Obviously, when the parameter λ is constant, system (29) can be integrated exactly. Thus, in system (29), $\lambda(t)$ is replaced by its initial value $\lambda(0)$, and the approximate solutions for the fraction are then computed as the exact solutions of the approximated sub-system:

$$\frac{\partial}{\partial t} (Y(t)) = \frac{\bar{Y}(\tau(0), e(0)) - Y(t)}{\lambda(0)}. \quad (30)$$

For an initial condition given by the value at time t^n , the final approximation at time $t^{n+1} = t^n + \Delta t^n$ then reads:

$$\left\{ \begin{array}{l} Y(t^{n+1}) = Y(t^n) e^{\frac{-\Delta t^n}{\lambda(t^n)}} + \bar{Y}(t^n) (1 - e^{\frac{-\Delta t^n}{\lambda(t^n)}}); \\ \rho(t^{n+1}) = \rho(t^n) \\ U(t^{n+1}) = U(t^n) \\ e(t^{n+1}) = e(t^n). \end{array} \right. \quad (31)$$

Remark 5. *It can easily be checked that when dealing with instantaneous thermodynamical relaxation, $\lambda(0) \rightarrow 0$, the scheme gives $Y(t^{n+1}) \rightarrow \bar{Y}(t^n)$. The associated thermodynamical states then correspond to the states that maximize the mixture entropy at $(\tau, e)(t^n)$. When $\bar{Y}(t^n) \in]0, 1[$, the pressure, temperature and chemical potential equilibria are ensured.*

Remark 6. *The update formula (31) for the fraction $Y(t^{n+1})$ is a barycenter between $Y(t^n)$ and $\bar{Y}(t^n)$. Hence, provided that $Y(t^n)$ and $\bar{Y}(t^n)$ lie in $[0, 1]^3$, $Y(t^{n+1})$ also lies in $[0, 1]^3$.*

4 Approximate solutions of Riemann problems

In this section, the numerical schemes of section 3 are assessed by the mean of Riemann Problems. For that purpose, Stiffened Gas EOS and the LuT of section 2 have been used. Considering the consistency of the schemes or the asymptotic rate of convergence, it could be sufficient to focus on Stiffened Gas EOS. Nevertheless, verification procedure can be seen as an unbiased tool to compare numerical schemes with respect to a known reference-solution. Different aspects can thus be compared as: the accuracy with respect to the mesh-size, the accuracy with respect to the CPU-time -which is very important for industrial applications-, the behavior for canonical solutions as isolated waves.

In the following, several Riemann problems are considered for the model of section 1. They are only composed of contact waves and shock waves. As depicted on figure (2), we consider: a ghost wave for the field $U - c$, a contact wave U and a shock wave $U + c$. Depending on the test case, the contact wave U and the shock $U + c$ may be ghost waves in order to study the accuracy of the schemes for isolated waves. The analytical rarefaction waves are far more complex to evaluate with accuracy when using the LuT, as depicted in appendix B. We do not consider these regular waves in the sequel.

Considering that the model of section 1 possesses a convective part and source terms that bring the system back to the thermodynamical equilibrium, “out-of-equilibrium” Riemann problems -with $\lambda \rightarrow \infty$ - and “at-equilibrium” Riemann problem -with $\lambda \rightarrow 0$ - are proposed. For out-of-equilibrium Riemann problems, only the convective part of the numerical procedure is considered. For the latter, the analytical solutions of the Riemann problem are computed using the mixture EOS for $Y = \bar{Y}$. In the simulation, we apply the whole scheme of section 3 based on a Lie-splitting: we first account for the convective terms with an out-of-equilibrium mixture EOS, and the thermodynamical equilibrium is then enforced through the source terms. The aim of these tests is to check the convergence of the relaxation approach for the simulation of cases where the mixture EOS is not regular (in particular the sound speed of the mixture EOS at-equilibrium).

The general setting of the Riemann problems is the following, see figure (2). We consider the one-dimensional domain $x \in [0 \ m, 1 \ m]$ and the initial discontinuity is located at $x_d = 1/2 \ m$. This domain is discretized using uniform meshes. The exact solution consists in the left and right initial states, respectively denoted by 1 and 3 on figure (2), separated by a uniform intermediate state, denoted by 2 on figure (2). When two ghost waves are imposed, the state 2 obviously coincides with the state 1 or 3. For each EoS, Stiffened Gas or LuT, we can compute the analytical solution of the Riemann problem. In the case of the LuT EoS, the initialization of each state must be done carefully because the LuT is defined on the (P, T) -plane and the use of an other plane may lead to a loss of accuracy. This is obviously not the case for Stiffened Gas EoS. The method used to compute the analytical solutions of the Riemann problem is classical. Several different test cases have been considered. The table 1 sums up their main characteristics and the initial data for

each test case are reported in appendix [D](#).

The analytical solutions are then used to compute the relative L^1 -error of the numerical approximations obtained with the different schemes. For an approximated solution Ψ^{approx} and an exact solution Ψ^{exact} , since the mesh size is uniform, the relative L^1 -error is computed at time t^n on the whole mesh as:

$$\frac{\sum_i |\Psi_i^{approx,n} - \Psi^{exact}(x_i, t^n)|}{\sum_i |\Psi^{exact}(x_i, t^n)|},$$

where x_i is the barycenter of the cell i . Obviously, when $\sum_i |\Psi^{exact}(x_i, t^n)| = 0$ this relative error is meaningless and we then consider the mere L^1 -error:

$$\sum_i |\Psi_i^{approx,n} - \Psi^{exact}(x_i, t^n)|.$$

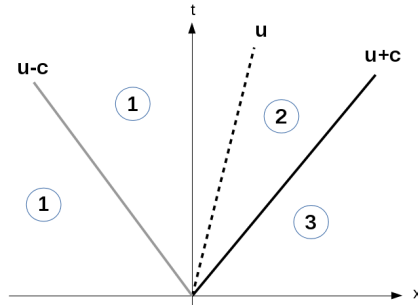


Figure 2: Riemann problem with one intermediate state; U-C: ghost wave; U: contact wave; U+C: shock wave

§	Waves	Eq. ?	EOS	Initial states Left/Right	Data
4.1	C + S	No	SG	liq. + vap. / liq. + vap.	D.1
4.1	C + S	No	LuT	liq. + vap. / liq. + vap.	D.1
4.2	C + S	Yes	LuT	liq. + vap. / liq. + vap.	D.2
4.3	C	Yes	LuT	liq. / liq. + vap.	D.3
4.3	S	Yes	LuT	liq. / liq. + vap.	D.4

Table 1: List of the presented test cases. In the second colmun, “C” stands for contact and “S” for shock. The third column ”Eq. ?” specifies if the EOS is at equilibrium (“Yes”), with $\lambda \rightarrow 0$, or out-of-equilibrium (“No”), with $\lambda \rightarrow +\infty$. The fourth column recalls the nature of the initial states (liquid, vapor or mixture). The last column refers to the appendix where initial data are given.

4.1 Out of equilibrium test cases for the Stiffened Gas EOS and the LuT

In this section, we investigate the behavior of the three schemes of section 3.1 for Riemann problems involving the out-of-equilibrium EOS. For both test cases we focus on the convective part and the source terms are not accounted for, i.e. $\lambda \rightarrow \infty$. The first Riemann problem is based on the Stiffened Gas EOS, whereas the second one involved the mixture EOS using the LuT. Since these two Riemann problems only involve a contact wave and a shock wave, it is possible to choose the same left states and the same intermediate states. The right states have then been chosen so that the right densities are equal. Obviously, since the Stiffened Gas EOS and the LuT are different for the right pressures, the right velocities and the shock speeds are different.

We first want to point out that VFRoe-ncv scheme fails during the very first iterations on the test case with the LuT. lie outside the domain of definition of the LuT. section 2. Rusanov scheme and the relaxation scheme are not subject to these drawbacks and are thus more robust while using the LuT. As a consequence, only Rusanov scheme and the relaxation scheme have been used with the LuT in the following. For the Stiffened Gas EOS, the three numerical schemes have been tested.

4.1.1 Asymptotic rate of convergence

The convergence curves at time $t_{end} = 2.5 \cdot 10^{-4} s$ are plotted on figure (3a) for the Stiffened Gas EOS and on figure (3b) for the LuT. Since we are dealing with Riemann problems that involve linearly degenerate waves and genuinely non-linear waves, the asymptotic rate of convergence should be $1/2$. Indeed, this order $1/2$ is reached for the volume fraction α (the behavior is the same for the three fractions) on the finest mesh for all schemes in both cases: all the other quantities will reach the same order with finer meshes.

When focusing on the Stiffened Gas test case (see figure (3a)), the relaxation scheme and VFRoe-ncv scheme have very similar behaviors and they are less diffusive than Rusanov scheme. This can be observed with the results for the fraction α . Considering the analytical solution, the fraction does not depend on the genuinely linear waves and it travels with the velocity of the contact wave which is equal to $1 m/s$ in our case (see appendix D.1). Hence at time $t_{end} = 2.5 \cdot 10^{-4} s$, the initial discontinuity on α has covered a distance of $L = 1 \times t_{end} = 2.5 \cdot 10^{-4} m$. As long as the size of a cell of the mesh is greater than L , the approximated contact will remain in the same cell during the simulation $t \in [0, t_{end}]$. So that the relative error with respect to the exact solution will not vary a lot. Since the logarithm (base 10) of L is equal to -3.6 , this explains the constant relative error for α on the coarse meshes on figure (3a) (i.e. for abscissa greater than -3.6). The same behavior occurs for the LuT test case with the relaxation scheme on figure (3b). This behavior is not observed here for Rusanov scheme because of its high level of numerical diffusion on the contact waves.

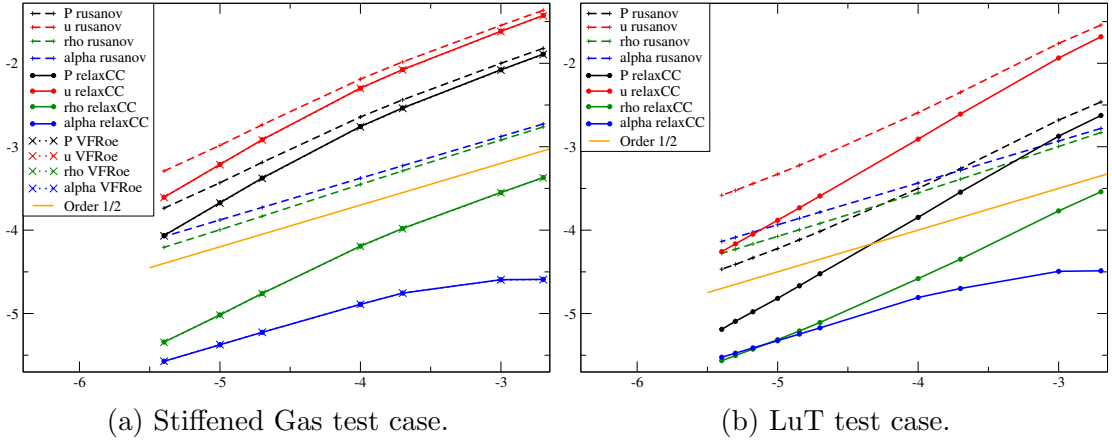


Figure 3: Convergence curves for the Riemann problems out of equilibrium: logarithm of the relative L^1 -error versus the logarithm of the mesh size with uniform meshes containing from 500 to 250 000 cells.. The error is plotted for the approximate solutions obtained with the different schemes and for P , U , ρ , α .

4.1.2 Accuracy and efficiency

Due to our choice for the analytical solutions, the profiles for P , U and α along the domain are uniform on each side of a traveling discontinuity:

- P and U only jump across the shock wave;
- α only jumps across the contact wave.

On the contrary, the density ρ has two jumps, one across the shock wave and one across the contact wave. Preservation of pressure or velocity through the contact wave is a well known problem; see for instance [45]. Moreover, it has been shown in [46] that preservation of constant values through a contact wave requires some constraints on the EOS depending on the numerical diffusivity of the numerical method. Here, due to the form of the mixture EOS of the studied model, it is not possible to get the same behavior on the approximated solutions for the contact wave, at least on coarse meshes. Indeed, U and P present spurious waves at the location of the contact wave. Even if these spurious waves tend to vanish when the mesh is refined (approximate solutions converge towards the analytical solution with $[U] = [P] = 0$ in the contact wave), the accuracy is influenced by these spurious waves. These waves can be observed on figure (8) of section 4.3.2.

For the two test cases, see figures (3a) and (3b), VFRoe-ncv scheme and the relaxation scheme provide a better accuracy than Rusanov scheme, at least for the density and the fractions, which strongly depend on the contact wave. The accuracy on the pressure and

on the velocity is only slightly improved for coarse meshes. Nevertheless, this improvement increases when the mesh is refined. This is due to the low velocity of the contact wave (1 m/s) and is related to the remark of the previous section. Indeed, as soon as the mesh is fine enough to provide an accurate approximation of the contact wave, the accuracy on pressure and the velocity increases because the spurious waves described above tend to vanish rapidly.

For the LuT test case, see figure (3b), we observe similar behavior: the relaxation scheme is far better than Rusanov scheme for the fractions and the density and the error is comparable for on U and P on coarse meshes. Moreover, the accuracy improvement with the relaxation scheme becomes more and more important when the mesh is refined.

On the figures (4a) and (4b), the error is plotted as a function of CPU-time in order to compare the schemes in term of efficiency. For a given CPU-time, the relaxation scheme gives the best accuracy for both EOS. When focusing on the Stiffened Gas test case, the relaxation scheme and VFRoe-scheme have a very similar efficiency (see figure 4a), with a slight advantage for the relaxation scheme. Indeed, the computation of VFRoe-ncv flux requires an additional thermodynamical computation. In the LuT test case, the efficiency gain with the relaxation scheme compared with Rusanov scheme is even more significant than in the Stiffened Gas test case. With the LuT, the number of thermodynamical computations is the same than with the stiffened gas EOS but each one is more CPU-time consuming. Rusanov scheme and the relaxation scheme require exactly the same calls to the LuT, but the gain in accuracy with the relaxation scheme allows to use coarser meshes. As a consequence, a given accuracy is then achieved with far less calls to the LuT with the relaxation scheme and CPU-time is thus saved.

4.2 At equilibrium test case: convection and relaxation effects

In this paragraph, a Riemann problem assuming thermodynamical equilibrium is considered (see appendix D.2). This means that the source terms are now taken into account: for each time-iteration, after the convection step, the fractions relax towards the equilibrium. We want to assess here the convergence rate of the Lie splitting described in section 3 with a source-term step that ensures the instantaneous relaxation towards the thermodynamical equilibrium. The Riemann problem considered here is composed of a contact wave and a $U + c$ shock wave. The convergence curves are presented on figure (5).

Since the numerical schemes used for the convection step have an asymptotic rate of convergence of $1/2$ (see section 4.1.1), since the source terms are discretized using a first order scheme in time and since the Lie splitting is a first order splitting, the asymptotic rate of convergence of the whole fractional step algorithm should be $1/2$. This order can be observed for Rusanov scheme when considering the fractions and the density. Nevertheless, the pressure and the velocity have not yet reached this asymptotic rate of convergence.

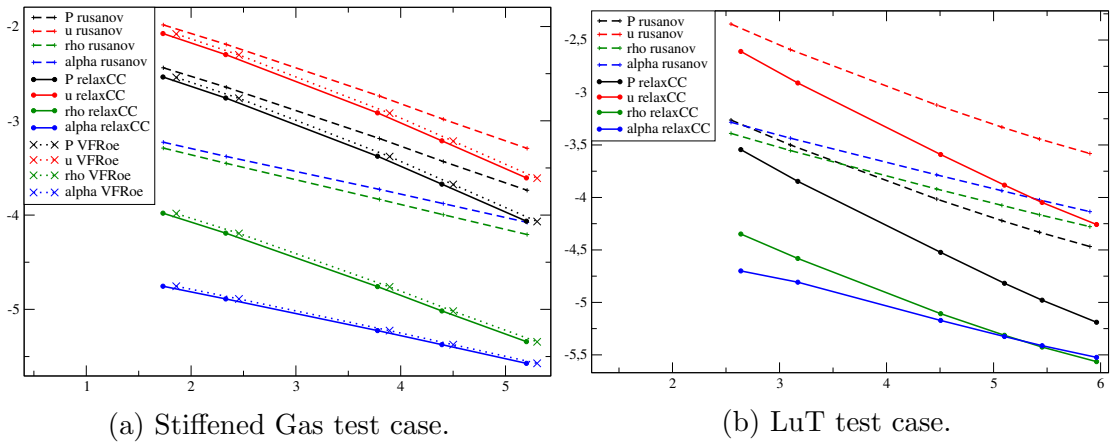


Figure 4: Comparison of the CPU-time for Riemann problems out of equilibrium with uniform meshes containing from 500 to 250 000 cells: logarithm of the relative L^1 -error versus the logarithm of the CPU-time. The error and CPU-time are plotted for the approximate solutions obtained with the different schemes and for P , U , ρ , α .

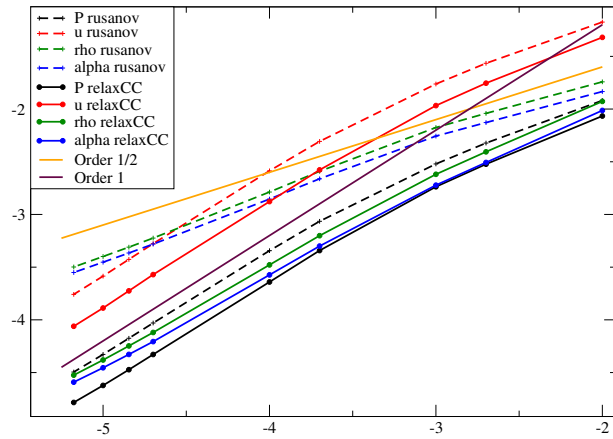


Figure 5: Convergence curve for the Riemann problems at equilibrium computed with the LuT: logarithm of the error versus logarithm of the mesh size. Four quantities are plotted: P , U , ρ , α for two different numerical schemes (Rusanov and relaxation). The meshes contain from 100 to 200 000 regular cells.

When turning to the numerical approximations obtained with the relaxation scheme, none of the variables has reached 1/2, even if the slopes of the curves for the density and the fractions tend to decrease on fine meshes.

4.3 At equilibrium test cases with a pure liquid initial state

Industrial applications provide a lot of situations in which vaporization occurs in a pure liquid domain. One is thus faced with the problem of computations that involve a pure liquid domain and a domain in which liquid and vapour coexist. We thus propose here Riemann problems at thermodynamical equilibrium, with a transition from pure liquid towards a mixture of liquid and vapour. Two Riemann problems are considered with a liquid left state and a right state composed of a mixture of liquid and vapour. Each of these two Riemann problems involves only one wave (see appendixes [D.3](#) and [D.4](#)):

1. for the first one we only consider a $U + c$ shock-wave;
2. for the second one we only consider a contact-wave.

The two other waves are then ghost waves. These cases are difficult to handle for the numerical schemes because the liquid thermodynamical behavior is very different from the mixture one. The transition through the single wave is thus associated with strong variations of the physical quantities, in particular considering the sound speed.

4.3.1 Shock-wave with a liquid left initial state

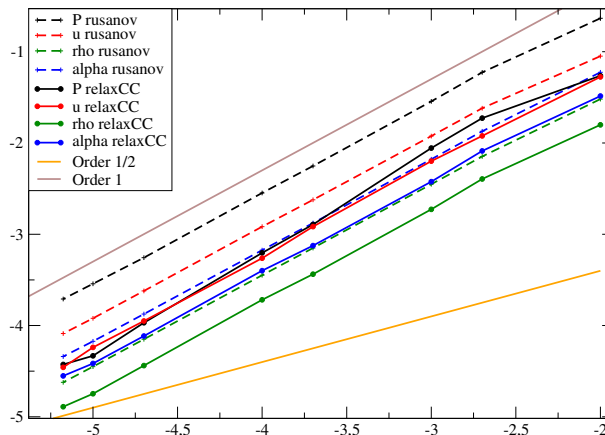


Figure 6: Convergence curve for a shock-wave: logarithm of the error versus logarithm of the mesh size. The left initial state is a pure liquid state and the right initial state is a mixture of liquid and vapour, both are at thermodynamical equilibrium. Four quantities are plotted: P , U , ρ , α . The meshes contain from 100 to 150 000 regular cells.

For this test case, the relaxation scheme was not robust enough and the computation stops in the very first iterations. In fact, in order to compute the fluxes between two cells, denoted by the subscripts r and l , the relaxation scheme uses an intermediate state with a modified pressure Π^* computed as:

$$\Pi^* = \frac{a}{2}(U_l - U_r) + \frac{1}{2}(\Pi_l + \Pi_r)$$

with the parameter

$$a^2 > \max\left(\frac{c_l}{\tau_l}, \frac{c_r}{\tau_r}\right).$$

In the present case, l is a liquid state and r a liquid-vapour mixture state (see appendix D.3). Hence $c_l/\tau_l \gg c_r/\tau_r$, and c_l/τ_l is very large, which leads to large parameter a . This has two drawbacks. First, the time-step is based on the value of a through the spectral radius and large values of a imply very small time-step. Moreover, since the difference between left and right initial velocities is not equal to zero, the pressure Π^* reaches too large values. Then the balance of the resulting numerical fluxes leads after few iterations to thermodynamical states that do not belong to the domain of definition of the LuT and the computation stops.

To overcome these difficulties, we have introduced a ‘‘Rusanov switch’’ into our code when computing the numerical fluxes with the relaxation scheme. Indeed, if the maximal eigenvalue computed with the parameter a is much greater than the maximal eigenvalue computed with Rusanov scheme, the relaxation numerical fluxes are replaced by the numerical fluxes obtained using Rusanov scheme. This modified version of the relaxation scheme is denoted in the following by the relaxation scheme with Rusanov switch. For the present test case, this switch only occurs on few cell-interfaces around the contact wave. For instance, for a mesh with 1000 cells, Rusanov switch only occurs for the interface at the middle of the domain during the first 12 time iterations.

The relaxation scheme with Rusanov switch is robust enough for the present test case. Since the switch only occurs on few cell-interfaces the accuracy of the relaxation scheme with Rusanov switch remains more accurate than Rusanov scheme. On the next test case, a comparison of Rusanov scheme, the relaxation scheme and the relaxation scheme with Rusanov switch is proposed.

4.3.2 Contact-wave with a liquid left state

For this test case (see D.4), the ‘‘relative’’ velocity at the shock location remains small and the relaxation scheme -without Rusanov switch- is robust enough. We are thus able to compare the results obtained with: Rusanov scheme, the relaxation scheme and the relaxation scheme with Rusanov switch. On figure (7), the error between the numerical approximations and the analytical solution is plotted with respect to the mesh size. The asymptotic convergence rate of $\frac{1}{2}$ is recovered for the finer meshes, even if Rusanov scheme needs very fine meshes to provide good approximations of the velocity. Moreover, the relaxation scheme enables a great improvement of the accuracy compared with Rusanov scheme: a little more than one order of magnitude on each quantity (see figure (7)). Indeed, Rusanov scheme creates large spurious waves around the contact wave as illustrated on figure (8). Some pressure oscillations are also created with the relaxation scheme and relaxation scheme with Rusanov switch, but their amplitude is a hundred times smaller. This behaviour is classical and it has been reported in [46].

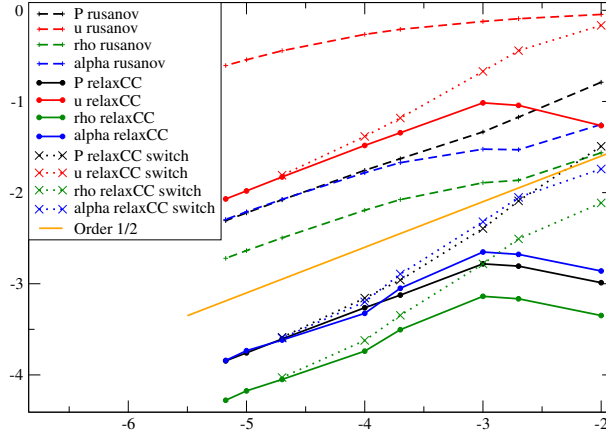


Figure 7: Convergence curve for a contact-wave: logarithm of the error versus logarithm of the mesh size. The left initial state is a pure liquid state and the right initial state is a mixture of liquid and vapour, both are at thermodynamical equilibrium. Four quantities are plotted: P , U , ρ , α . The meshes contain from 100 to 150 000 regular cells.

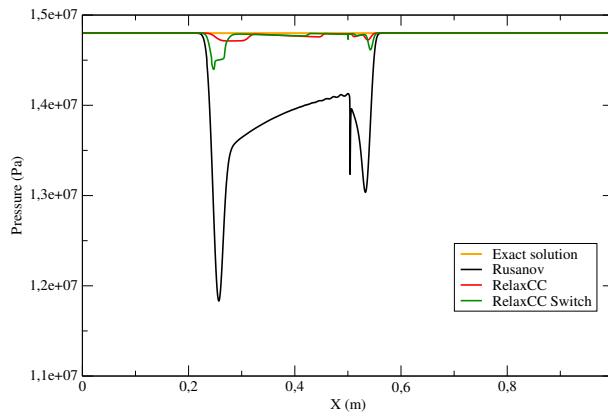


Figure 8: Pressure as a function of x at $t_{end} = 2.5 \cdot 10^{-4}$ s for a mesh with 5000 cells. The contact wave remains close to $x = 0.5$ and spurious numerical waves are created on both sides of the contact wave.

When focusing on the comparison of the relaxation scheme and the relaxation scheme with Rusanov switch, one can evaluate the loss of accuracy due to the switch with figure (7). It can be noted that the introduction of the switch reduces the accuracy of the relaxation scheme on coarse meshes but that this loss tends to vanish when the mesh is refined. Indeed, Rusanov switch only occurs on a few cell-interfaces and the loss of accuracy concerns an almost constant number of cell-interfaces **whatever the mesh size**

is. Hence, the more cells there are in the whole mesh, the less significant is the loss of accuracy due to Rusanov switch.

4.3.3 Conclusions for the at equilibrium test case with a liquid left state

In all cases, we have not encountered a loss of the asymptotic rate of convergence despite the sudden transition from liquid to two-phase flow. Nevertheless, the relaxation scheme is not always robust enough. This is the case for the shock-wave case proposed above. In order to tackle this loss of robustness the relaxation scheme with Rusanov switch as been tested when the parameter a arising from the Whitham condition becomes too high. This modification is applied only on a few cell-interfaces, the loss of accuracy is thus limited to coarse meshes, as it has been illustrated with the contact-wave case. However, it should be noted that even on very coarse meshes, the relaxation scheme with Rusanov switch provides a better accuracy than Rusanov scheme.

4.4 Conclusions

- When considering Stiffened Gas equation-of-state, the relaxation scheme is as accurate and efficient as VFRoe-ncv scheme. Unfortunately, VFRoe-ncv scheme described in section 3.1.2 is not robust enough when using the LuT. For the LuT, using an accurate scheme as the relaxation scheme enables to consider coarser meshes than with Rusanov scheme. This leads to fewer computations of the thermodynamical quantities for a given accuracy, and thus to far less expensive computations of the approximated solutions.
- Nevertheless, for the most severe cases, the relaxation scheme described in section 3.1.3 may fail. The relaxation scheme with Rusanov switch is robust enough for such cases and enables to keep a correct accuracy level.
- Verification test-cases are possible even with a complex equation of state and it allows to assess the behaviour of different schemes for canonical situations. The test-cases proposed above involve sudden phase transition from liquid to a two-phase flow, and the source terms have been accounted for considering equilibrium situations. Indeed, analytical solutions of the system with non-instantaneous thermodynamical relaxation are far more complex to exhibit.

5 Validation case: study of vaporization near a wall due to a rarefaction wave

Our model aims to simulate some accidental scenarii, like a LOCA scenario. The SUPERCANON experiment [40] is an experimental device representative of this scenario: a tube contains pressurized liquid water at $T = 573.15K$ and $P = 150 \text{ bar}$. The surrounding room contains air at atmospheric pressure $P = 1 \text{ bar}$. The cap is opened at the beginning of the experiment. The pressure then drops until a value close to the saturation pressure at $T = 573.15K$. This first pressure wave is a rarefaction wave that travels with a high speed in the liquid. When the rarefaction wave reaches the closed-end of the tube, vaporization begins and is strongly influenced by out of equilibrium effects. In the model of the section 1, these effects are ruled by the relaxation time λ chosen by the user. A study has been realized in [25], using toy laws for the relaxation time: it appears that the arrival of the first rarefaction wave on the wall and the first vaporization of the liquid due to the pressure drop are very sensitive to the choice of the closure law for λ . Experiments [40] also present various behaviors for a same experimental set up, which might be explained by the quantity of impurities in the liquid.

In this last section, we study a more simple case: vaporization near a wall due to a sudden pressure drop in the liquid. The aim is to focus on two types of relaxation time laws: constant values for this characteristic time scale as well as closure laws based on the nucleation theory have been tested. For the latter, we study a simplified model with only two parameters.

5.1 Presentation of the test case

We consider a tube filled with liquid water at $P=150 \text{ bar}$ and $T=593.15K$, closed on the left and open on the right (see figure 9). The initial fluid velocity is imposed at $+10 \text{ m/s}$: it induces a depressurization wave at the wall, which propagates towards the right outlet. When pressure decreases at the wall, vapor appears : the same phenomenon can be observed in the SUPERCANON experiment. This case can also be schematic of what happens downstream a valve closed abruptly in a pipe in which flows high pressurized water

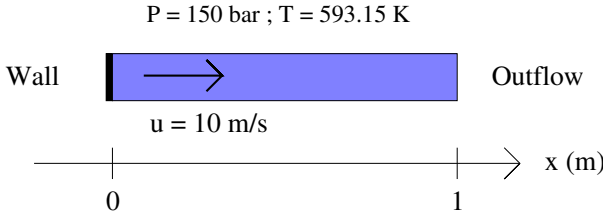


Figure 9: Sketch of the validation test case: depressurization wave in out-going liquid

5.2 Simple model for relaxation time based on Nucleation Theory

Nucleation refers to the apparition of the first new phase nuclei during a first order phase transition. A classical assumption (see for instance [37]) is that the bubble nucleation rate J (the number of bubbles created per unit time in unit volume) follows an Arrhenius law:

$$J = J_0 \exp\left(-\frac{E_a}{k_B T}\right), \quad (32)$$

where k_B is the Boltzmann constant, T is the liquid temperature, J_0 is a prefactor and E_a is an activation energy. From this nucleation rate J , we propose a simplified model for a time scale t_{nuc} characterizing the nucleation. From assumptions made for instance in [38] or [39], we define:

$$t_{nuc} = \left(\frac{a_0}{\Delta P}\right)^3 \exp\left(\frac{\varphi E_a}{k_B T}\right), \quad (33)$$

where E_a is defined by (85): $E_a = \frac{16\pi\gamma^3}{3(\Delta P)^2}$, and γ is estimated with the IAPWS 94 correlation [47]. $\varphi \in [0, 1]$ depends on the nucleation type : homogeneous nucleation occurs when $\varphi = 1$; whereas heterogeneous nucleation occurs when φ is in $]0, 1[$. The whole approach to get this simplified model as well as the chosen correlation for γ , are described in appendix C.

In the simplified model (33), we have only two parameters to define: a_0 in (Pa.s), homogeneous to a dynamical viscosity, and $\varphi \in [0, 1]$. Even if it is not a complete realistic model, it describes two important physical effects :

- Thanks to the Arrhenius law, heterogeneous nucleation only begins if a minimal energy barrier is reached;
- Dependance on $\frac{1}{\Delta P^3}$ reflects a physical behaviour which seems relevant: when $\Delta P \rightarrow \infty$, the return towards thermodynamical equilibrium becomes instantaneous; whereas when $\Delta P \simeq 1$, the return towards equilibrium may require a finite time, which enables the persistence of out-of-equilibrium states for small ΔP .

5.3 Numerical results

In the following simulations, the domain is $[0, 1]$, the mesh contains 5000 cells and the final time is 10^{-3} s. Empirically, we observe that, according to the CFL condition and the mesh size, the time step is almost constant, around $5 \cdot 10^{-8}$ s.

5.3.1 Constant relaxation times

Constant relaxation times have first been considered. Although they are probably not physically relevant, they enable to illustrate how out of equilibrium effects can change or not the solution.

The difference between pressure (P) and saturation pressure (P_{sat}) near the wall is plotted on figure 10. Because of water moving to the right of the tube, a rarefaction wave appears at the wall, travelling to the right: pressure then decreases, until it reaches the saturation pressure. After that, vaporization may occur.

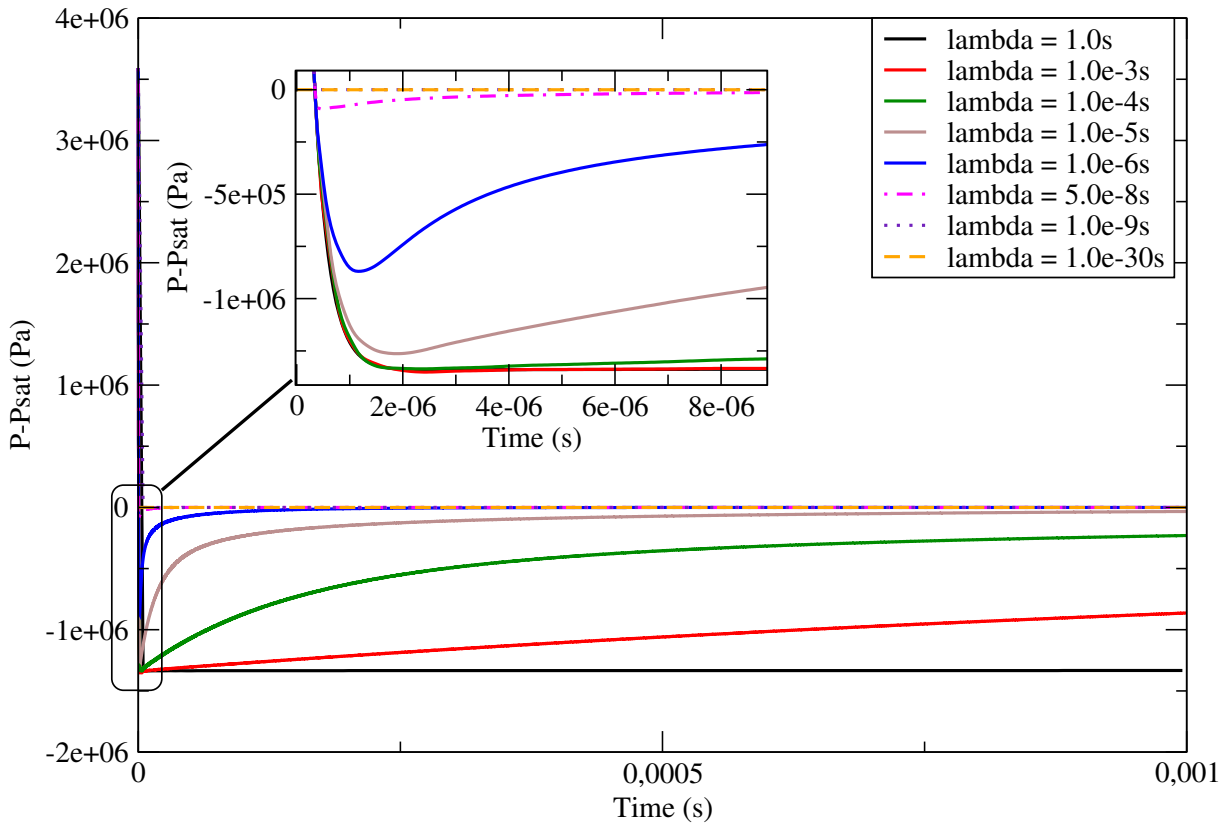


Figure 10: Difference between the pressure and the saturation pressure near the wall as a function of time (s) for several constant relaxation times. The second window inside the first graph shows a zoom on the beginning of the simulation for the smaller relaxation times.

When relaxation time tends to zero (case ' $\lambda = 10^{-30}$ s'), thermodynamical equilibrium is instantaneously reached: it means that $P = P_{sat}$ during the whole simulation. In fact, as soon as the relaxation time is small enough, pressure almost directly decreases to reach the saturation pressure and remains constant at this value during the whole simulation.

However, when the relaxation time is high, a pressure undershoot appears at the very beginning of the simulation: the pressure decreases below the saturation pressure, which postpones the beginning of the vaporization. The higher λ is, the more the pressure decreases. Indeed, high relaxation times prevent from reaching the thermodynamical equilibrium: the vaporization can not occur and the flow remains liquid. Without phase change, the only possibility to release energy of the rarefaction wave for the system is to reduce the pressure. After the first brutal drop, pressure increases rather slowly towards the saturation pressure, depending on the time scale λ .

On figure 11, pressure and volume fraction are plotted with respect to x at the end of the simulation ($t = 10^{-3}$ s). For small relaxation times, vapor creation is located at the left side of the tube, whereas vapor is more spread throughout the tube when the relaxation time is high. The pressure undershoot is more important when λ is high.

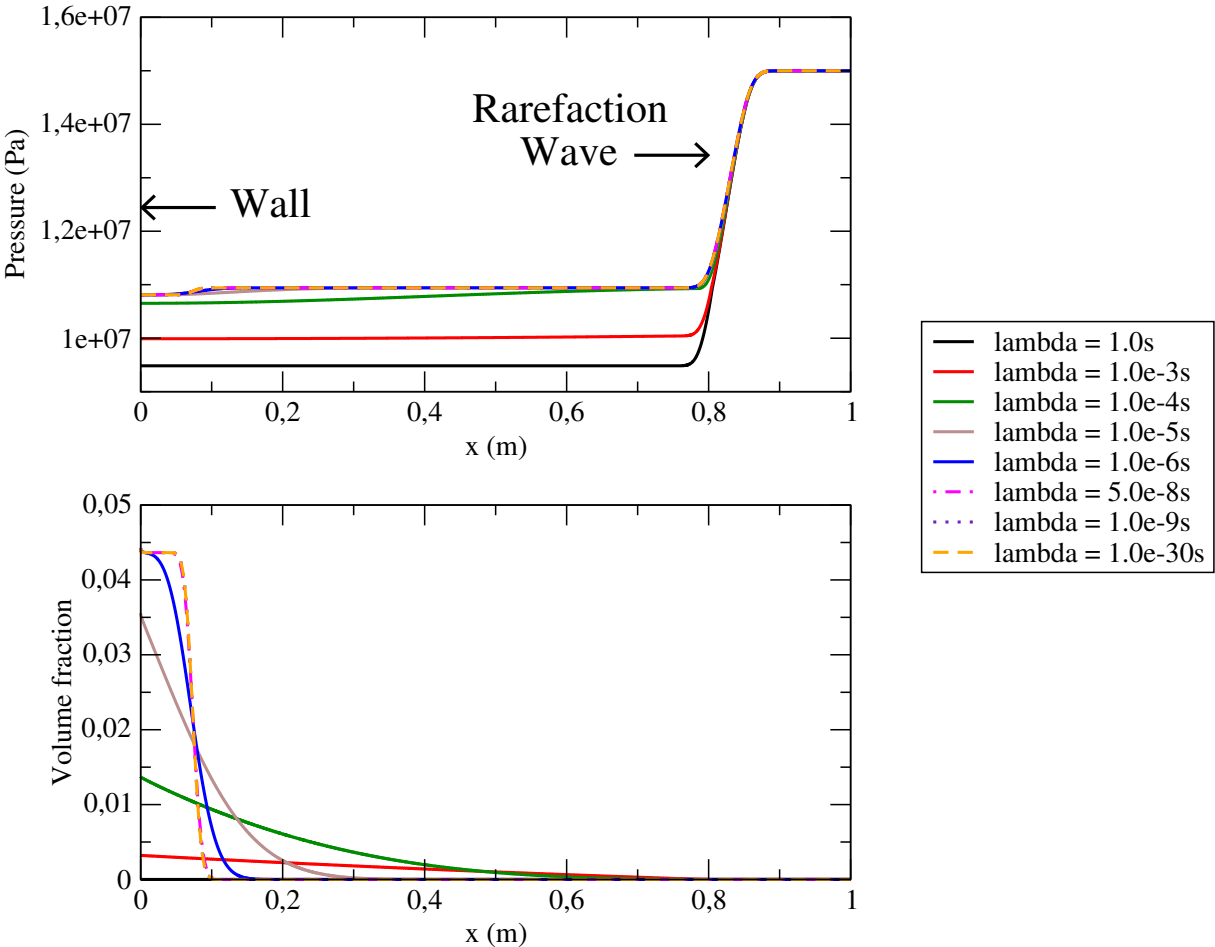


Figure 11: Pressure (Pa) and volume fraction as a function of x (m) for several constant relaxation times at the end of the simulation ($t=10^{-3}$ s).

5.3.2 Relaxation times based on nucleation theory

In this part, we take $\lambda = t_{nuc}$ as expressed by (33). Two parameters have to be chosen: a_0 and φ .

- For this first study, we fix $a_0 = 1.7 \cdot 10^5$ Pa.s. This choice is not based on physical argument. Remembering the order of magnitude of ΔP in the simulation of section 5.3.1, this value of a_0 empirically gives λ with the same order of magnitude than the time step. The idea here is to study the behaviour of the exponential term in t_{nuc} .
- Several φ have thus been tested: $\varphi \in \{1; 6.5 \cdot 10^{-3}; 5 \cdot 10^{-3}; 3.3 \cdot 10^{-3}; 5 \cdot 10^{-4}; 1 \cdot 10^{-4}\}$. We recall that homogeneous nucleation occurs when $\varphi = 1$; when heterogeneous nucleation occurs, φ is in $]0, 1[$.

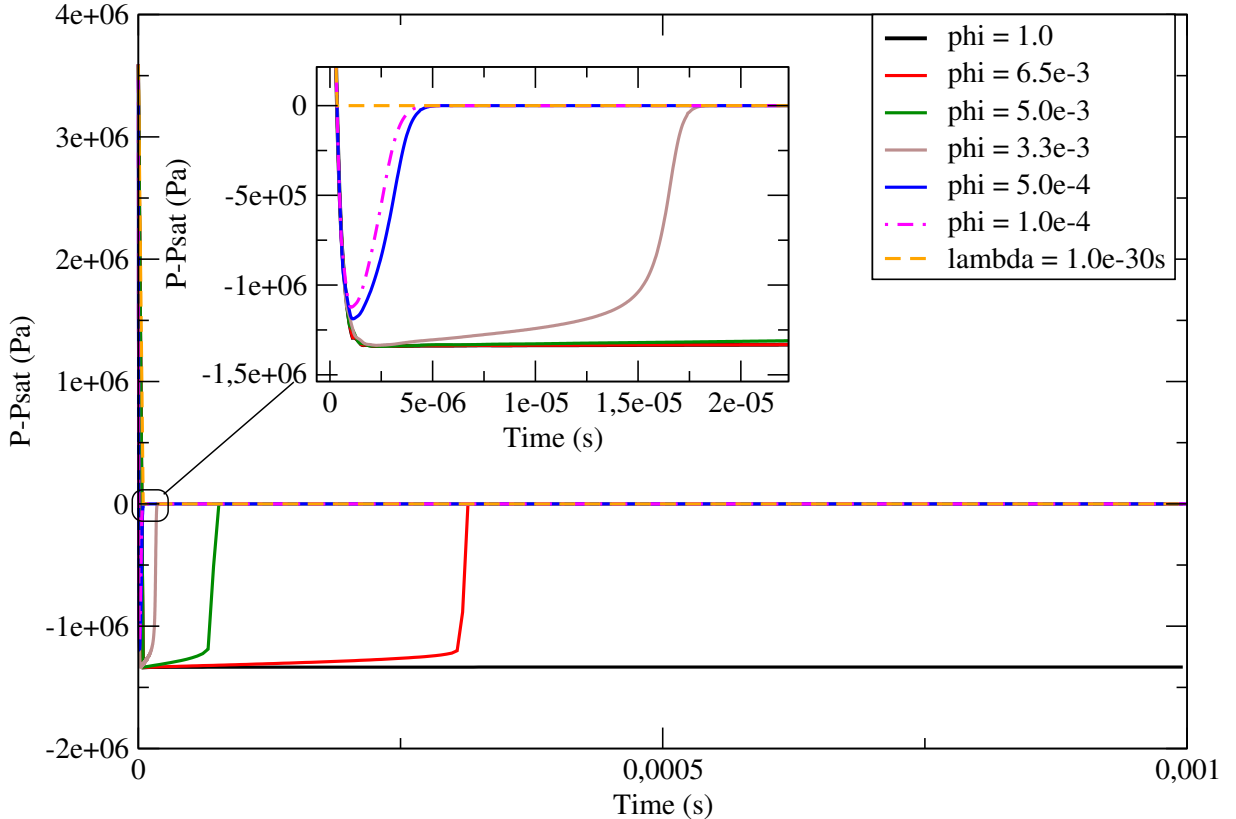


Figure 12: Difference between the pressure and the saturation pressure near the wall as a function of time (s) for several nucleation relaxation times, with fixed a_0 and variable φ . The more φ is closed to 0, the more nucleation is facilitated. The second window inside the first graph shows a zoom on the beginning of the simulation for relaxation times with $\varphi \rightarrow 0$.

On figure 12, the difference $P - P_{sat}$ (Pa) is plotted as a function of the time t (s) near the wall. A violent pressure undershoot below the saturation pressure occurs at the

very beginning of the simulation. When nucleation is completely homogenous ($\varphi = 1$), the pressure stays almost constant and far below saturation pressure: this case is very similar to the case with constant and very high relaxation time ($\lambda = 1$ s', see figure 10). With a homogeneous nucleation, E_a is thus high and does not allow to create bubbles. The parameter φ that tends to decrease this energy then plays an important role. The magnitude of the undershoot slightly vary with φ : the more heterogeneous nucleation is ($\varphi \rightarrow 0$), the lower the pressure undershoot is. In fact, the parameter φ has a greater influence on the duration of the pressure undershoot than on its magnitude.

On figure 13, pressure and volume fraction are plotted at the end of the simulation with respect to x : by comparison with the simulations with constant λ , the stiffness of the Arrhenius term in t_{nuc} (33) leads to complex behaviors for the pressure drop. Some oscillations occur for $x \simeq 0.05$ m, around the frontier between the pure liquid domain and the two-phase domain. These oscillations are numerically stable and tend to vanish when the mesh is refined. Last, it can be observed that the relaxation time law based on nucleation theory modifies the vapor creation: contrary to constant relaxation times (see figure 11), a greater amount of vapor appears in a more localized area close to the wall (see figure 13).

Finally, changing the relaxation time laws leads to a change of the thermodynamical path towards thermodynamical equilibrium. Several behaviors of the mixture are observed depending on the chosen relaxation time law. They are summed up on figure 14:

- an initial strong pressure undershoot without return towards equilibrium before the simulation ends ($\lambda = 1$ s' or 'Nucleation, $\varphi = 1.0$ ');
- a mixture staying almost at thermodynamical equilibrium during the whole simulation ($\lambda = 5.0 \cdot 10^{-8}$ s');
- an initial strong pressure undershoot with smooth return towards thermodynamical equilibrium ($\lambda = 1.0 \cdot 10^{-5}$ s');
- an initial strong pressure undershoot with jumps throughout T-P plane ('Nucleation with $\varphi = 5.0 \cdot 10^{-3}$ ' or 'Nucleation with $\varphi = 1.0 \cdot 10^{-4}$).

Even if our simplified nucleation model is not completely physical in its current form, this study shows how strongly relaxation time laws can modify mixture behavior throughout the simulation.

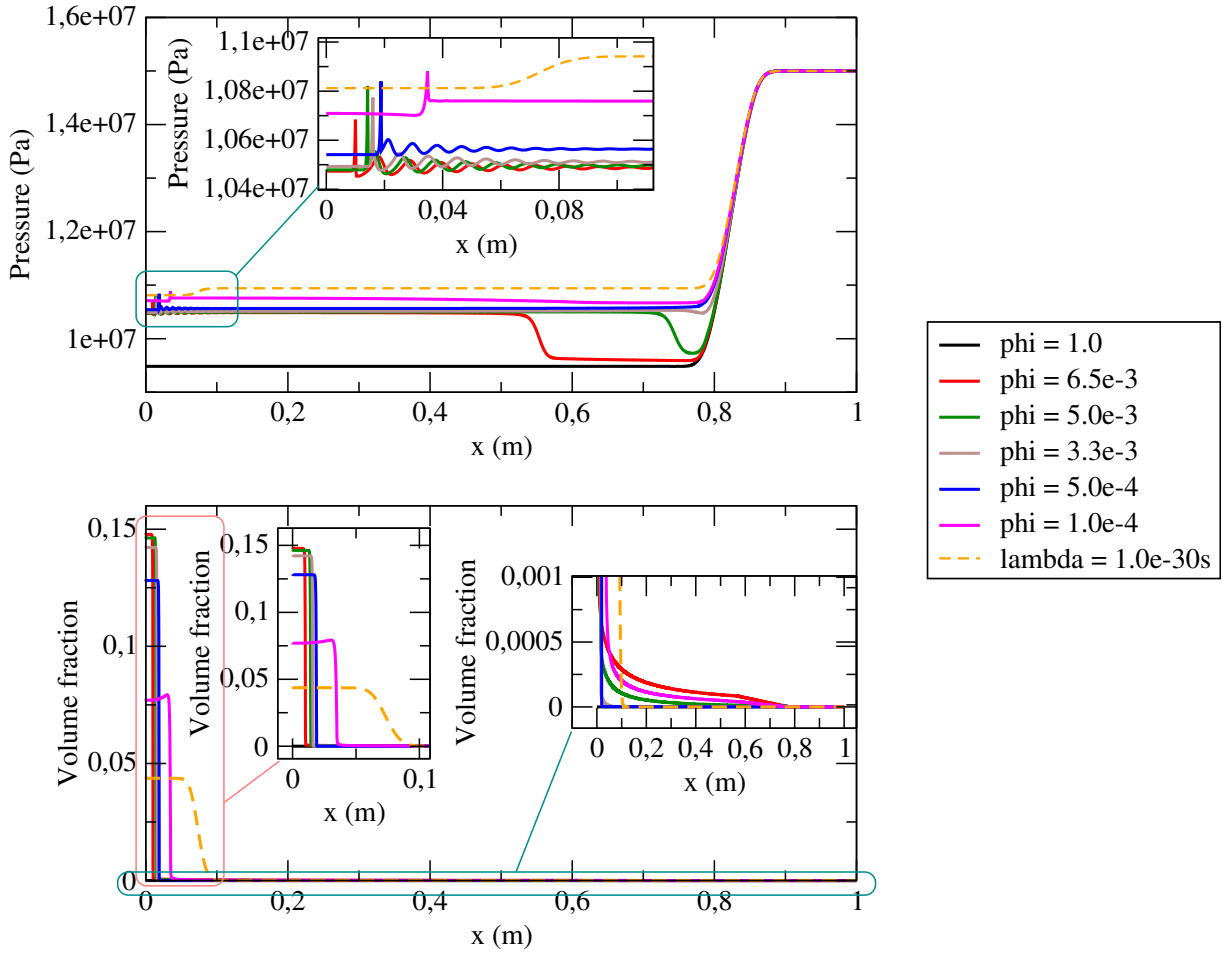


Figure 13: Pressure (Pa) and volume fraction as a function of x (m) for several relaxation times based on nucleation theory at the end of the simulation ($t=10^{-3}$ s). The two smaller windows inside the main graph are two zooms: one on the smaller x , the other on the smaller volume fractions.

Conclusion

The homogeneous model of section 1 has been used with a complex equation of state based on the look-up table (LuT) of section 2. This LuT allows to save computation time with respect to the direct use of the IAPWS-97 formulation (computations with the LuT are 90 times faster) and provides more realistic values than a classical analytical EOS as the Stiffened Gas on a wide range of pressure and temperature. In a numerical point of view, the relaxation scheme proposed in [32] has been implemented and its behaviour has been assessed on different Riemann problems involving both a Stiffened Gas EOS and the look-up table described in section 2. This relaxation scheme provides a great accuracy and a very satisfactory robustness, which are both mandatory when using industrial look-up tables. In section 5, the influence of the time-scale λ that rules the return to the ther-

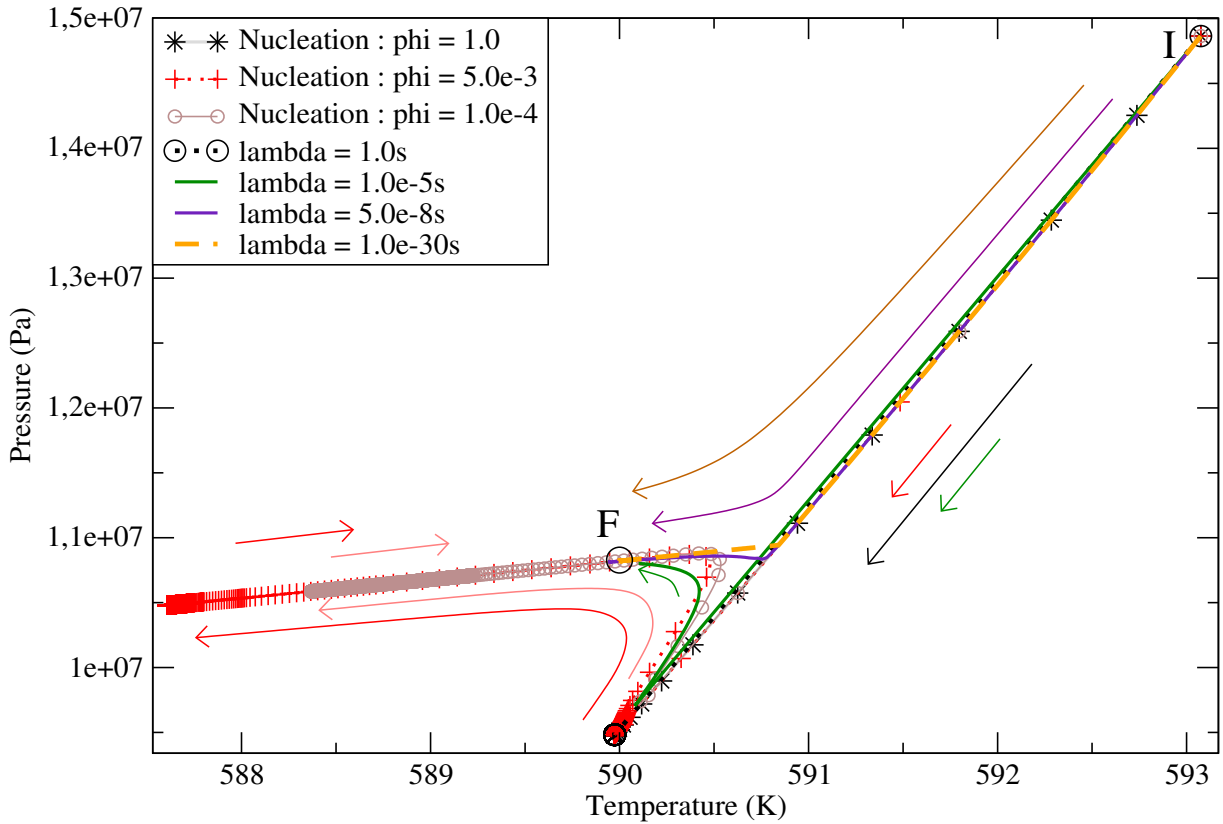


Figure 14: Thermodynamical path within the time near the wall is plotted in the Temperature (K) - Pressure (Pa) plane. The initial point for all curves is on the hand-right corner (denoted by the circle I). The thermodynamical equilibrium (denoted by the circle F) is the point that all simulations should reach for large enough time, provided that $\lambda > 0$. If $\lambda = 0$, the final point is the point $P = 9.4810^6 Pa$ $T = 589 K$ at the bottom of the figure. Here some simulations are still out of thermodynamical equilibrium at the final simulation time $t = 10^{-3} s$. The paths towards thermodynamical equilibrium depends on the characteristic time-scale λ . Arrows show the travel directions in the T-P plane along the simulation time.

modynamical equilibrium has been investigated: various values of λ have been compared to a very simple - yet non-linear - model based on the nucleation theory. The results are very interesting and this work should be pursued by performing some comparisons on the basis of relevant out-of-equilibrium experiments. Moreover, the nucleation theory includes surface tension effects and a further improvement of the present work could be to include in the model both the interfacial area and the surface tension effects.

Acknowledgements

The last author receives financial support by ANRT through an EDF/CIFRE grant number 2017/0476. Computational facilities were provided by EDF. The authors thank the reviewers for their helpful remarks, improving the paper structure.

Appendix

A Building of the homogeneous model

In this section, we build step by step a homogeneous model to describe a mixture of liquid and vapour, by considering at first the extensive variables [48], as made in [16, 19, 20, 21, 22]. The only equilibrium assumption in the model is a kinematic equilibrium. In particular, the model enables to describe the mixture out of the thermodynamical equilibrium. The return to equilibrium is ensured by a relaxation process in agreement with the second law of thermodynamics.

A.1 Extensive description of the system

Three extensive quantities are needed to describe a two-phase mixture [48]. Let us consider a volume \mathcal{V} (in m^3) of the mixture, corresponding to a mass \mathcal{M} (in kg) and an internal energy \mathcal{E} (in J). Within this mixture, each phase $k = l, v$ is described with the same quantities: a volume \mathcal{V}_k (in m^3), a mass \mathcal{M}_k (in kg) and an energy \mathcal{E}_k (in J).

Some assumptions are made:

- (H_1) The geometric repartition of the phases inside the volume V is not taken into account.
- (H_2) The surface tension is neglected.
- (H_3) The whole volume \mathcal{V} is occupied by some fluid (vacuum occurrence is not considered here).
- (H_4) The phases are **not miscible**.

With these assumptions, we can easily express the conservation of volume, mass and energy as:

$$\mathcal{V} = \mathcal{V}_l + \mathcal{V}_v \quad ; \quad \mathcal{M} = \mathcal{M}_l + \mathcal{M}_v \quad ; \quad \mathcal{E} = \mathcal{E}_l + \mathcal{E}_v. \quad (34)$$

The hypothesis (H_3) and (H_4) are mandatory to write the first equation of (34) on the volumes. When dealing with the miscible case (i.e. when (H_4) is not fulfilled), one can for instance make the assumption that the two phases occupy the whole volume. In such a case, the first equation of (34) is replaced by two equations describing the equality of the volumes, $\mathcal{V} = \mathcal{V}_l = \mathcal{V}_v$, which leads to another system of equations. This case does

not enter the scope of the present work and it has been investigated in details in [17, 18, 49].

The aim is now to describe the evolution of this system in accordance with the first and second laws of thermodynamics and Newton's laws of dynamics. We proceed in two steps by adopting a lagrangian point of view. In section 1.2 and 1.3 we first consider the thermodynamical behavior of a fixed quantity of mixture. For this purpose we follow a classical approach [21, 22] based on the evolution of a closed and isolated mass of mixture in agreement with the second law of thermodynamics. Then, in section 1.4, we account for the evolution of this mass of mixture within the whole flow by applying the first law of thermodynamics and Newton's law.

A.2 Thermodynamical quantities

A.2.1 Kinematic equilibrium

The kinematic equilibrium between the phases is assumed, i.e.:

(H_5) both phases are convected with the same velocity U .

Thanks to this assumption of equal velocity ($U_l = U_v = U$), the dynamical behavior of the system can be described by modelling the behavior of an element $(\mathcal{V}, \mathcal{M}, \mathcal{E})$ of the mixture along a streamline. In particular, since $U_k = U$, the derivative along a streamline of phase k of a quantity Φ ,

$$d_k \Phi = (\partial_t \Phi + U_k \partial_x \Phi) dt,$$

corresponds to the same operator for both phases. So that the derivative along a streamline does not depend on the indice k :

$$d_k \Phi = (\partial_t \Phi + U \partial_x \Phi) dt = d\Phi. \quad (35)$$

This last equation (35) is a key relation which will enable us to simply derive the model.

A.2.2 Phasic thermodynamical quantities

In order to close the system, we need to define a complete EOS for each phase. For this purpose, we assume that each phase is described by an extensive entropy $(W_k) \mapsto S_k(W_k)$ (in J/K), where we have set $W_k = (\mathcal{V}_k, \mathcal{M}_k, \mathcal{E}_k)$. Some hypotheses are needed on S_k to guarantee usefull properties for the final model:

(H_6) $(W_k) \mapsto S_k(W_k)$ is \mathcal{C}^2 .

(H_7) $(W_k) \mapsto S_k(W_k)$ is concave.

(H_8) $\forall a \in \mathbb{R}^+, \forall W_k, S_k(aW_k) = aS_k(W_k)$.

(H_9) $\forall W_k, \frac{\partial S_k}{\partial \mathcal{E}_k} > 0$

In agreement with the Classical Irreversible Thermodynamics (CIT) theory, the classical Gibbs relation holds for each phase:

$$T_k d_k \mathcal{S}_k = d_k \mathcal{E}_k + P_k d_k \mathcal{V}_k - \mu_k d_k \mathcal{M}_k. \quad (36)$$

Thanks to (35), it can be rewritten as:

$$T_k d\mathcal{S}_k = d\mathcal{E}_k + P_k d\mathcal{V}_k - \mu_k d\mathcal{M}_k. \quad (37)$$

The extensive entropy S_k using the variables $(\mathcal{V}_k, \mathcal{M}_k, \mathcal{E}_k)$ is a complete EOS for phase k when associated with the Gibbs relation (37). This means that all the thermodynamical quantities can be computed thanks to the derivatives of S_k :

$$\frac{P_k}{T_k} = \left. \frac{\partial S_k}{\partial \mathcal{V}_k} \right|_{\mathcal{M}_k, \mathcal{E}_k} \quad (38)$$

$$\frac{1}{T_k} = \left. \frac{\partial S_k}{\partial \mathcal{E}_k} \right|_{\mathcal{V}_k, \mathcal{M}_k} \quad (39)$$

$$\frac{\mu_k}{T_k} = - \left. \frac{\partial S_k}{\partial \mathcal{M}_k} \right|_{\mathcal{V}_k, \mathcal{E}_k} \quad (40)$$

where P_k is the pressure of phase k (in Pa), T_k (in K) is the temperature of phase k , and μ_k (in J/kg) is the Gibbs free enthalpy of phase k .

A.2.3 Thermodynamical quantities of the mixture

We note $W = (\mathcal{V}_l, \mathcal{M}_l, \mathcal{E}_l, \mathcal{V}_v, \mathcal{M}_v, \mathcal{E}_v) = (W_l, W_v)$. Thanks to (H_2) , we assume that the entropy of the mixture S is:

$$(W) \mapsto S(W) = S_l(W_l) + S_v(W_v) \quad (41)$$

This mixture entropy should be defined using another relation if surface tension (or other effects, see [7]) had to be accounted for.

We define $\mathcal{H}(\mathcal{M})$, a subset of $(\mathbb{R}_+^*)^6$ so that all the states $W \in \mathcal{H}(\mathcal{M})$ have the same total mass \mathcal{M} :

$$\mathcal{H}(\mathcal{M}) = \{W \in (\mathbb{R}_+^*)^6; \mathcal{M}_l + \mathcal{M}_v = \mathcal{M}\}.$$

If the entropy S is concave thanks to the definition (41) and properties (H_5) and (H_7) , it can be proved that S is strictly concave on $\mathcal{H}(\mathcal{M})$ (see [18, 21, 22]).

Using the Gibbs relation for each phase (37), the definition of the mixture entropy (41) and relation (35), a Gibbs relation for the mixture can be easily exhibited:

$$\begin{aligned} d\mathcal{S} &= d\mathcal{S}_l + d\mathcal{S}_v = \frac{1}{T_l} d\mathcal{E}_l + \frac{1}{T_v} d\mathcal{E}_v \\ &+ \frac{P_l}{T_l} d\mathcal{V}_l + \frac{P_v}{T_v} d\mathcal{V}_v - \frac{\mu_l}{T_l} d\mathcal{M}_l - \frac{\mu_v}{T_v} d\mathcal{M}_v \end{aligned} \quad (42)$$

Thanks to the relation $d\Phi_k = \Phi d\left(\frac{\Phi_k}{\Phi}\right) + \frac{\Phi_k}{\Phi}d\Phi$, Gibbs relation (42) for the mixture can be written in the form:

$$\begin{aligned}
dS &= \left(\frac{\mathcal{E}_l}{\mathcal{E}} \frac{1}{T_l} + \frac{\mathcal{E}_v}{\mathcal{E}} \frac{1}{T_v}\right) d\mathcal{E} + \left(\frac{\mathcal{V}_l}{\mathcal{V}} \frac{P_l}{T_l} + \frac{\mathcal{V}_v}{\mathcal{V}} \frac{P_v}{T_v}\right) d\mathcal{V} \\
&- \left(\frac{\mathcal{M}_l}{\mathcal{M}} \frac{\mu_l}{T_l} + \frac{\mathcal{M}_v}{\mathcal{M}} \frac{\mu_v}{T_v}\right) d\mathcal{M} \\
&+ \mathcal{E} \frac{1}{T_l} d\left(\frac{\mathcal{E}_l}{\mathcal{E}}\right) + \mathcal{E} \frac{1}{T_v} d\left(\frac{\mathcal{E}_v}{\mathcal{E}}\right) \\
&+ \mathcal{V} \frac{P_l}{T_l} d\left(\frac{\mathcal{V}_l}{\mathcal{V}}\right) + \mathcal{V} \frac{P_v}{T_v} d\left(\frac{\mathcal{V}_v}{\mathcal{V}}\right) \\
&- \mathcal{M} \frac{\mu_l}{T_l} d\left(\frac{\mathcal{M}_l}{\mathcal{M}}\right) - \mathcal{M} \frac{\mu_v}{T_v} d\left(\frac{\mathcal{M}_v}{\mathcal{M}}\right)
\end{aligned} \tag{43}$$

Then, using relation (43), we can identify a mixture pressure P , a mixture temperature T and a mixture Gibbs free enthalpy μ :

$$\frac{P}{T} = \frac{\mathcal{V}_l}{\mathcal{V}} \frac{P_l}{T_l} + \frac{\mathcal{V}_v}{\mathcal{V}} \frac{P_v}{T_v} \tag{44}$$

$$\frac{1}{T} = \frac{\mathcal{E}_l}{\mathcal{E}} \frac{1}{T_l} + \frac{\mathcal{E}_v}{\mathcal{E}} \frac{1}{T_v} \tag{45}$$

$$\frac{\mu}{T} = \frac{\mathcal{M}_l}{\mathcal{M}} \frac{\mu_l}{T_l} + \frac{\mathcal{M}_v}{\mathcal{M}} \frac{\mu_v}{T_v}. \tag{46}$$

and we thus get the Gibbs relation:

$$\begin{aligned}
&dS - \frac{1}{T} (d\mathcal{E} + Pd\mathcal{V} - \mu d\mathcal{M}) \\
&= \mathcal{E} \frac{1}{T_l} d\left(\frac{\mathcal{E}_l}{\mathcal{E}}\right) + \mathcal{V} \frac{P_l}{T_l} d\left(\frac{\mathcal{V}_l}{\mathcal{V}}\right) - \mathcal{M} \frac{\mu_l}{T_l} d\left(\frac{\mathcal{M}_l}{\mathcal{M}}\right) \\
&+ \mathcal{E} \frac{1}{T_v} d\left(\frac{\mathcal{E}_v}{\mathcal{E}}\right) + \mathcal{V} \frac{P_v}{T_v} d\left(\frac{\mathcal{V}_v}{\mathcal{V}}\right) - \mathcal{M} \frac{\mu_v}{T_v} d\left(\frac{\mathcal{M}_v}{\mathcal{M}}\right)
\end{aligned} \tag{47}$$

The terms on the left-hand side of this relation define the evolution of the mixture quantities and are related to the interaction with the surrounding fluid, whereas the terms on the right-hand side are exchange terms between the phases. In order to give a complete time-evolution model of our system, we need to express the derivative terms of (47) in terms of W .

A.3 Modelling exchange terms between the phases

Let us first focus on the exchange terms in (47). We thus consider an isolated amount of mixture so that: $d\mathcal{E} = d\mathcal{V} = d\mathcal{M} = 0$. In other words, we consider a subset $\mathcal{D}(\mathcal{V}, \mathcal{M}, \mathcal{E})$ of $\mathcal{H}(\mathcal{M})$ so that all the states $W \in \mathcal{D}(\mathcal{V}, \mathcal{M}, \mathcal{E})$ have the same total volume \mathcal{V} , the same total mass \mathcal{M} and the same total energy \mathcal{E} :

$$\mathcal{D}(\mathcal{V}, \mathcal{M}, \mathcal{E}) = \{W \in \mathcal{H}(\mathcal{M}) ; \mathcal{V}_l + \mathcal{V}_v = \mathcal{V} ; \mathcal{E}_l + \mathcal{E}_v = \mathcal{E}\}.$$

In order to respect the second law of thermodynamics, the mixture entropy S of such an isolated system must increase. As a consequence, the models for $d(\mathcal{V}_k/\mathcal{V})$, $d(\mathcal{M}_k/\mathcal{M})$ and $d(\mathcal{E}_k/\mathcal{E})$ must be chosen so that $dS \geq 0$.

The Gibbs relation (47) becomes for such an isolated system:

$$\begin{aligned} dS &= \mathcal{E} \frac{1}{T_l} d\left(\frac{\mathcal{E}_l}{\mathcal{E}}\right) + \mathcal{V} \frac{P_l}{T_l} d\left(\frac{\mathcal{V}_l}{\mathcal{V}}\right) - \mathcal{M} \frac{\mu_l}{T_l} d\left(\frac{\mathcal{M}_l}{\mathcal{M}}\right) \\ &+ \mathcal{E} \frac{1}{T_v} d\left(\frac{\mathcal{E}_v}{\mathcal{E}}\right) + \mathcal{V} \frac{P_v}{T_v} d\left(\frac{\mathcal{V}_v}{\mathcal{V}}\right) - \mathcal{M} \frac{\mu_v}{T_v} d\left(\frac{\mathcal{M}_v}{\mathcal{M}}\right) \end{aligned} \quad (48)$$

As in [16], we assume that the time-evolution of these quantities are of the form:

$$(H_8) \quad \begin{cases} d\left(\frac{\mathcal{V}_k}{\mathcal{V}}\right) = \frac{\bar{\mathcal{V}}_k - \mathcal{V}_k}{\lambda \mathcal{V}} dt, \\ d\left(\frac{\mathcal{M}_k}{\mathcal{M}}\right) = \frac{\bar{\mathcal{M}}_k - \mathcal{M}_k}{\lambda \mathcal{M}} dt, \\ d\left(\frac{\mathcal{E}_k}{\mathcal{E}}\right) = \frac{\bar{\mathcal{E}}_k - \mathcal{E}_k}{\lambda \mathcal{E}} dt, \end{cases} \quad (49)$$

with $\lambda > 0$. The state $\bar{W} = (\bar{\mathcal{V}}_l, \bar{\mathcal{M}}_l, \bar{\mathcal{E}}_l, \bar{\mathcal{V}}_v, \bar{\mathcal{M}}_v, \bar{\mathcal{E}}_v)$ then corresponds to the state that the system will asymptotically reach. Let us define \bar{W} so that models (49) comply with the second law of thermodynamics.

By differentiating the mixture entropy S with respect to the variable W , we get:

$$dS = \nabla_W(S)(W).dW. \quad (50)$$

Since we have an isolated system, $d\mathcal{V} = d\mathcal{M} = d\mathcal{E} = 0$, which implies:

$$\begin{aligned} dW &= \left(\mathcal{V} d\left(\frac{\mathcal{V}_l}{\mathcal{V}}\right), \mathcal{M} d\left(\frac{\mathcal{M}_l}{\mathcal{M}}\right), \mathcal{E} d\left(\frac{\mathcal{E}_l}{\mathcal{E}}\right), \right. \\ &\quad \left. \mathcal{V} d\left(\frac{\mathcal{V}_v}{\mathcal{V}}\right), \mathcal{M} d\left(\frac{\mathcal{M}_v}{\mathcal{M}}\right), \mathcal{E} d\left(\frac{\mathcal{E}_v}{\mathcal{E}}\right) \right) \end{aligned} \quad (51)$$

From (49), (50) and (51) it follows that:

$$dS = \nabla_W(S). \left(\frac{\bar{W} - W}{\lambda} \right) dt. \quad (52)$$

Since S is strictly concave on $\mathcal{H}(\mathcal{M})$, it is also strictly concave on $\mathcal{D}(\mathcal{V}, \mathcal{M}, \mathcal{E})$. This property implies that the tangent plane to S at any point W of $\mathcal{H}(\mathcal{M})$ is above S :

$$\forall W_0 \in \mathcal{H}(\mathcal{M}), S(W_0) \leq S(W) + \nabla_W(S)(W).(W_0 - W). \quad (53)$$

In particular, we can write the concavity condition (53) for $W_0 = \bar{W}$, which leads to:

$$\nabla_W(S)(W).(\bar{W} - W) \geq S(\bar{W}) - S(W)$$

so that from (52) we get:

$$dS \geq \frac{(S(\bar{W}) - S(W))}{\lambda} dt. \quad (54)$$

As a consequence, **one possible choice** to guarantee the growth of the entropy with the models (49) is to define the state \bar{W} as the point which maximizes the mixture entropy for a fixed $(\mathcal{V}, \mathcal{M}, \mathcal{E})$:

$$S(\bar{W}) = \max_{\mathcal{D}(\mathcal{V}, \mathcal{M}, \mathcal{E})} (S(W)) \quad (55)$$

Thanks to the strict concavity of S on $\mathcal{D}(\mathcal{V}, \mathcal{M}, \mathcal{E})$, this point exists and is unique. Hence, with the definition (55) for the state \bar{W} , the growth of the mixture entropy of an isolated system is ensured by the models (49).

Moreover, Gibbs relation (48) on $\mathcal{D}(\mathcal{V}, \mathcal{M}, \mathcal{E})$ can be simplified by using relations (34). Indeed, when focusing on the volume relation in (34), we have:

$$\begin{aligned} \sum_k d\left(\frac{\mathcal{V}_k}{\mathcal{V}}\right) &= \sum_k \left(\left(\frac{d\mathcal{V}_k}{\mathcal{V}} \right) - \mathcal{V}_k \left(\frac{d\mathcal{V}}{\mathcal{V}^2} \right) \right) \\ &= \frac{d(\sum_k \mathcal{V}_k)}{\mathcal{V}} - (\sum_k \mathcal{V}_k) \left(\frac{d\mathcal{V}}{\mathcal{V}^2} \right) = 0 \end{aligned}$$

Obviously, the same results can be obtained for masses and energies, so that we have the following relations:

$$\begin{aligned} d\left(\frac{\mathcal{V}_l}{\mathcal{V}}\right) &= -d\left(\frac{\mathcal{V}_v}{\mathcal{V}}\right); \\ d\left(\frac{\mathcal{M}_l}{\mathcal{M}}\right) &= -d\left(\frac{\mathcal{M}_v}{\mathcal{M}}\right) \quad ; \quad d\left(\frac{\mathcal{E}_l}{\mathcal{E}}\right) = -d\left(\frac{\mathcal{E}_v}{\mathcal{E}}\right). \end{aligned} \quad (56)$$

Eventually, by introducing relations (56) in Gibbs relation (48), we obtain the following relation on $\mathcal{D}(\mathcal{V}, \mathcal{M}, \mathcal{E})$:

$$\begin{aligned} dS &= \mathcal{E} \left(\frac{1}{T_l} - \frac{1}{T_v} \right) d\left(\frac{\mathcal{E}_l}{\mathcal{E}}\right) + \mathcal{V} \left(\frac{P_l}{T_l} - \frac{P_v}{T_v} \right) d\left(\frac{\mathcal{V}_l}{\mathcal{V}}\right) \\ &\quad - \mathcal{M} \left(\frac{\mu_l}{T_l} - \frac{\mu_v}{T_v} \right) d\left(\frac{\mathcal{M}_l}{\mathcal{M}}\right) \end{aligned} \quad (57)$$

Since the mixture entropy is strictly concave on $\mathcal{D}(\mathcal{V}, \mathcal{M}, \mathcal{E})$, it possesses a unique maximum \bar{W} on $\mathcal{D}(\mathcal{V}, \mathcal{M}, \mathcal{E})$. If this maximum is not reached on the boundary of $\mathcal{D}(\mathcal{V}, \mathcal{M}, \mathcal{E})$, the derivative of S with respect to $\mathcal{V}_l/\mathcal{V}$, $\mathcal{M}_l/\mathcal{M}$ and $\mathcal{E}_l/\mathcal{E}$ must vanish at \bar{W} . The latter is thus defined by the following relations:

$$\begin{cases} P_l(\bar{\mathcal{V}}_l, \bar{\mathcal{M}}_l, \bar{\mathcal{E}}_l) = P_v(\bar{\mathcal{V}}_v, \bar{\mathcal{M}}_v, \bar{\mathcal{E}}_v) \\ T_l(\bar{\mathcal{V}}_l, \bar{\mathcal{M}}_l, \bar{\mathcal{E}}_l) = T_v(\bar{\mathcal{V}}_v, \bar{\mathcal{M}}_v, \bar{\mathcal{E}}_v) \\ \mu_l(\bar{\mathcal{V}}_l, \bar{\mathcal{M}}_l, \bar{\mathcal{E}}_l) = \mu_v(\bar{\mathcal{V}}_v, \bar{\mathcal{M}}_v, \bar{\mathcal{E}}_v) \end{cases} \quad (58)$$

When the maximum is reached on the boundary of $\mathcal{D}(\mathcal{V}, \mathcal{M}, \mathcal{E})$, system (58) does not make sense since the derivatives of the mixture entropy do not vanish inside $\mathcal{D}(\mathcal{V}, \mathcal{M}, \mathcal{E})$.

Such situations correspond to single-phase cases for which W_1 or W_2 is equal to $(0, 0, 0)$.

The modelling of the evolution of the phasic volumes, phasic masses and phasic energies (49) enforces the system to return to the equilibrium state \bar{W} , which corresponds to the classical thermodynamical equilibrium state. The latter is defined as the state ensuring the pressure, temperature and Gibbs enthalpy equilibria (58). It has been shown in this section that these source terms (49) comply with the second law of the thermodynamics provided that the relaxation time-scale λ is chosen non-negative.

A.4 Dynamical evolution of the mixture quantities

The previous subsection describes a model for the evolution of each phase of an element $(\mathcal{V}, \mathcal{M}, \mathcal{E})$ isolated from the rest of the fluid. The interaction between the surrounding fluid and the the mixture described by the variables $(\mathcal{V}, \mathcal{M}, \mathcal{E}, U)$ is now considered by using the following classical assumptions:

(H_{10}) the mass \mathcal{M} is conserved along the streamlines:

$$d\mathcal{M} = 0; \quad (59)$$

(H_{11}) the variation of the volume \mathcal{V} is due to the divergence of the velocity field U :

$$d\mathcal{V} = \mathcal{V}\nabla_x \cdot (U)dt; \quad (60)$$

(H_{12}) the variation of the velocity U follows the Newton's law, considering here that only the forces due to the pressure are accounted for:

$$d(\mathcal{M}U) = -\mathcal{V}\nabla_x(P)dt, \quad (61)$$

where P corresponds to the mixture pressure defined by (44);

(H_{13}) the first law of thermodynamics applies to the energy \mathcal{E} :

$$d\mathcal{E} = -Pd\mathcal{V} + Qdt; \quad (62)$$

it means that the variation of \mathcal{E} is due to the work of the external forces (only the pressure forces here) and to the heat exchange Q of the system with its surroundings.

Remark 7. Thanks to assumptions (H_{10}) and (H_{13}), with $Q = 0$, we have $d\mathcal{E} + Pd\mathcal{V} - \mu d\mathcal{M} = 0$. Hence the general Gibbs relation (47) reduces to the Gibbs relation for a isolated system (57).

A.5 The set of Partial Derivative Equations (PDE) in intensive form

From now the system has been described using extensive variables. Indeed, extensive variables provide a more comprehensive description of the model. But, since our aim is to build a set of partial derivative equations, it is convenient to use an intensive description of the system. In this section, we derive the extensive description of the two-phase flow of the previous sections into an intensive description.

A.5.1 Fractions and phasic specific quantities

The mass conservation assumption (H_{10}) enables to define specific quantities (per unit of mass). The specific volume of the mixture is thus defined as $\tau = \mathcal{V}/\mathcal{M}$ (in m^3/kg), and the specific energy of the mixture is $e = \mathcal{E}/\mathcal{M}$ (in J/kg). We recall the notations for the volume fraction α_k , the mass fraction y_k and the energy fraction z_k of phase k :

$$Y_k = (\alpha_k, y_k, z_k) = \left(\frac{\mathcal{V}_k}{\mathcal{V}}, \frac{\mathcal{M}_k}{\mathcal{M}}, \frac{\mathcal{E}_k}{\mathcal{E}} \right) \quad (63)$$

The phasic specific volume and the phasic specific energy of phase k are then:

$$\begin{aligned} \tau_k &= \frac{\mathcal{V}_k}{\mathcal{M}_k} = \frac{\mathcal{V}_k}{\mathcal{V}} \frac{\mathcal{M}}{\mathcal{M}_k} \frac{\mathcal{V}}{\mathcal{M}} = \frac{\alpha_k}{y_k} \tau; \\ e_k &= \frac{\mathcal{E}_k}{\mathcal{M}_k} = \frac{\mathcal{E}_k}{\mathcal{E}} \frac{\mathcal{M}}{\mathcal{M}_k} \frac{\mathcal{E}}{\mathcal{M}} = \frac{z_k}{y_k} e. \end{aligned} \quad (64)$$

The conservation equations (34) become:

$$1 = \alpha_l + \alpha_v \quad ; \quad 1 = y_l + y_v \quad ; \quad 1 = z_l + z_v. \quad (65)$$

The thermodynamical evolution equation (49) can be written:

$$d\alpha_k = \frac{\bar{\alpha}_k - \alpha}{\lambda} dt; \quad dy_k = \frac{\bar{y}_k - y_k}{\lambda} dt; \quad dz_k = \frac{\bar{z}_k - z_k}{\lambda} dt \quad (66)$$

where $\bar{Y}_k = (\bar{\alpha}_k, \bar{y}_k, \bar{z}_k) = \left(\frac{\bar{V}_k}{V}, \frac{\bar{M}_k}{M}, \frac{\bar{E}_k}{E} \right)$ denotes the equilibrium fractions.

A.5.2 Specific mixture entropy and Gibbs relation

Let us define the mass \mathcal{M}_k as $\mathcal{M}_k = \mathcal{M}'_k \mathbb{I}_{kg}$, where \mathbb{I}_{kg} is equal to 1 kg and $\mathcal{M}'_k \in \mathbb{R}^+ - \{0\}$ is dimensionless. By denoting s_k the specific entropy of phase k , $s_k = S_k/\mathcal{M}_k$, and by using the property (H_8), we have:

$$s_k \left(\frac{X_k}{\mathcal{M}_k} \right) = \frac{S_k(X_k, \mathcal{M}_k)}{\mathcal{M}_k} = \frac{1}{\mathbb{I}_{kg}} S_k \left(\frac{X_k}{\mathcal{M}'_k}, \frac{\mathcal{M}_k}{\mathcal{M}'_k} \right) = \frac{1}{\mathbb{I}_{kg}} S_k \left(\frac{X_k}{\mathcal{M}'_k}, \mathbb{I}_{kg} \right).$$

where X_k stands here for $(\mathcal{V}_k, \mathcal{E}_k)$. We thus get the link between extensive and intensive quantities:

$$s_k \left(\frac{X_k}{\mathcal{M}_k} \right) = \frac{1}{\mathbb{I}_{kg}} S_k \left(\frac{X_k}{\mathcal{M}'_k}, \mathbb{I}_{kg} \right) = \frac{S_k(X_k, \mathcal{M}_k)}{\mathcal{M}_k} \quad (67)$$

The specific mixture entropy can be defined as:

$$\forall W \in \mathcal{H}(\mathcal{M}), \mathcal{M} > 0, s \left(\frac{W}{\mathcal{M}} \right) = \frac{S(W)}{\mathcal{M}}. \quad (68)$$

By using the relation (67) for the phasic entropies we get the expression of the specific mixture entropy:

$$\begin{aligned} s \left(\frac{W}{\mathcal{M}} \right) &= \frac{S_l(W_l)}{\mathcal{M}} + \frac{S_v(W_v)}{\mathcal{M}} = \frac{\mathcal{M}_l}{\mathcal{M}} \frac{S_l(W_l)}{\mathcal{M}_l} + \frac{\mathcal{M}_v}{\mathcal{M}} \frac{S_v(W_v)}{\mathcal{M}_v} \\ &= \frac{\mathcal{M}_l}{\mathcal{M}} s_l \left(\frac{X_l}{\mathcal{M}_l} \right) + \frac{\mathcal{M}_v}{\mathcal{M}} s_v \left(\frac{X_v}{\mathcal{M}_v} \right). \end{aligned}$$

The mixture entropy s can finally be re-written using the fractions of phase l :

$$s(\alpha_l, y_l, z_l, \tau, e) = y_l s_l \left(\frac{\alpha_l}{y_l} \tau, \frac{z_l}{y_l} e \right) + (1 - y_l) s_v \left(\frac{(1 - \alpha_l)}{(1 - y_l)} \tau, \frac{(1 - z_l)}{(1 - y_l)} e \right)$$

In the same way, the Gibbs relation for the mixture can be written using the intensive quantities:

$$\begin{aligned} ds &= \frac{1}{T} de + \frac{P}{T} d\tau + \tau \left(\frac{P_l}{T_l} - \frac{P_v}{T_v} \right) d\alpha_l \\ &\quad - \left(\frac{\mu_l}{T_l} - \frac{\mu_v}{T_v} \right) dy_l + e \left(\frac{1}{T_l} - \frac{1}{T_v} \right) dz_l \end{aligned} \quad (69)$$

where the mixture temperature and the mixture pressure are:

$$\begin{aligned} \frac{1}{T} &= z_l \frac{1}{T_l(\tau_l, e_l)} + z_v \frac{1}{T_v(\tau_v, e_v)}; \\ \frac{P}{T} &= \alpha_l \frac{P_l(\tau_l, e_l)}{T_l(\tau_l, e_l)} + \alpha_v \frac{P_v(\tau_v, e_v)}{T_v(\tau_v, e_v)}. \end{aligned} \quad (70)$$

A.5.3 Intensive PDE in a one dimensional framework

The equations (59), (61), (62) can be written with intensive quantities:

$$\begin{cases} d\tau = \tau \nabla_x \cdot (U) dt \\ dU = -\tau \nabla_x \cdot (P) dt \\ de = -P d\tau + q dt \end{cases} \quad (71)$$

where $q = Q/M$, the specific heat-power is set to zero in the following:

$$q = 0. \quad (72)$$

Let us note the mixture density:

$$\rho = 1/\tau, \quad (73)$$

the specific total energy of the mixture:

$$E = e + |U|^2/2, \quad (74)$$

and the vector gathering the fractions:

$$Y = (\alpha_l, y_l, z_l)^t. \quad (75)$$

By using the relation (35), which states that:

$$d\Phi = (\partial_t \Phi + U \partial_x \Phi) dt, \quad (76)$$

it can be shown that the set of derivative equations (71) and (66) lead to the set of partial differential equations in conservative form:

$$\begin{cases} \frac{\partial}{\partial t} (\rho Y) + \frac{\partial}{\partial x} (\rho U Y) = \rho \Gamma, \\ \frac{\partial}{\partial t} (\rho) + \frac{\partial}{\partial x} (\rho U) = 0, \\ \frac{\partial}{\partial t} (\rho U) + \frac{\partial}{\partial x} (\rho U^2 + P) = 0, \\ \frac{\partial}{\partial t} (\rho E) + \frac{\partial}{\partial x} (U(\rho E + P)) = 0. \end{cases} \quad (77)$$

The system (77) is closed with the relations (64), (65), (70), and the source terms are:

$$\Gamma = \left(\frac{\bar{\alpha}_l - \alpha_l}{\lambda}, \frac{\bar{y}_l - y_l}{\lambda}, \frac{\bar{z}_l - z_l}{\lambda} \right).$$

The time-scale $\lambda > 0$ describing the return to the thermodynamical equilibrium has to be chosen by the user.

Remark 8. *Following the remark 1 of section 1.4, Gibbs relation for intensive quantities (69) becomes*

$$ds = \tau \left(\frac{P_l}{T_l} - \frac{P_v}{T_v} \right) d\alpha_l - \left(\frac{\mu_l}{T_l} - \frac{\mu_v}{T_v} \right) dy_l + e \left(\frac{1}{T_l} - \frac{1}{T_v} \right) dz_l. \quad (78)$$

The mixture entropy s is then convected with the velocity U , and subjected to the source terms Γ :

$$\frac{\partial}{\partial t} (\rho s) + \frac{\partial}{\partial x} (\rho U s) = \rho \Gamma \nabla_Y (s)|_{\tau, e}. \quad (79)$$

B Reference solution for a rarefaction wave with the LuT

Let us consider a single phase flow with a complex EOS, for instance in the form of the LuT proposed in the article. In the following we deal with a $u - c$ rarefaction wave, but the conclusions would obviously be the same for a $u + c$ rarefaction wave. For any point $*$ in a $u - c$ rarefaction wave separating a left state L and a right state R , the Riemann invariants are constant, which means in our case that:

$$s^* = s^L, \quad \text{and} \quad u^* + \int_{P_L}^{P^*} \frac{dP}{\rho c(s_0, P)} = u^L. \quad (80)$$

When using simple analytical EOS, as Stiffened Gas EOS for instance, the integral in the second condition of (80) can be explicitly computed. It is also easy to compute an isentropic path, which corresponds to the first condition of (80). Finally for such simple EOS, the definition of a point in the rarefaction wave relies on a local implicit computation (through a Newton algorithm or a dichotomy for instance) for system (80). The latter can be done up to the round-off error of the computer.

With our complex EOS based on the (P, T) plane, the isentropic path can only be approximated from the left state to the right state using Newton-like algorithm. Moreover, the integral arising in the second condition of (80) can not be explicitly written. It must also be approximated using classical integration algorithm along the isentropic path. We have thus two sources of numerical approximation in the definition of the thermodynamical path of the rarefaction wave.

On the other hand, our particular choice for the polynomials (cubic splines) of the LuT leads to an even more important drawback. Indeed, as depicted above, we can approximate the rarefaction wave in the thermodynamical plane (P, T) using numerical algorithms, but we are not able to project this thermodynamical path onto the (t, x) plane. A point $*$ of the $u - c$ rarefaction wave is connected to the point (t, x^*) thanks to the relation:

$$\frac{x^* - x_0}{t} = u^* - c^*.$$

Since the rarefaction wave is a regular wave between two time-space points (t, x^L) and (t, x^R) , $u^* - c^*$ has to be continuous and monotonic to allow a regular projection. It should then be noted that the sound speed c can be written with respect to the second order derivatives of μ :

$$c^2 = \left(\frac{\chi_T}{\tau} - \frac{T\alpha_P^2}{C_p} \right)^{-1}, \quad (81)$$

where

$$C_p = -T \left. \frac{\partial^2 \mu}{\partial T^2} \right|_P; \quad \alpha_p = \frac{1}{\tau} \left. \frac{\partial^2 \mu}{\partial p \partial T} \right|_{T,p}; \quad \chi_T = \frac{1}{\tau} \left. \frac{\partial^2 \mu}{\partial p^2} \right|_T. \quad (82)$$

Since our LuT is based on cubic splines, it only ensures a \mathcal{C}^1 μ , but we can not ensure the continuity of c between to neighboring cells of the LuT. We are thus not able to perform the projection of the rarefaction wave from the thermodynamical plane (P, T) to the (t, x) plane.

Finally, due to our complex EOS, we could only perform a weak comparison between the approximated solution given by our code and an approximated rarefaction wave in the thermodynamical (P, T) -plane. This comparison is weak in the sense that we would get a “reference” rarefaction wave obtained through a numerical integration and not an analytical one. In order to perform this weak comparison in the (t, x) plane, we should use a higher polynomial basis instead of the splines, so that the sound speed would be continuous and monotonic on the whole domain.

We propose here to build a “reference” solution for a $u - c$ rarefaction wave as depicted above. We consider initial data such that the left state is a pressurized liquid state and the right state is pure vapor at saturation (see table 2). The quantities e , ρ and $\phi_2 = \int_{P_L}^{P^*} \frac{dP}{\rho c(s_0, P)}$ are continuous and they have been plotted on figures 15, 16 and 17 with respect to the pressure. The quantity $\xi^* = \frac{x^* - x_0}{t} = u^* - c^*$ is plotted on figure 18, the non-monotonic behavior associated to c can be clearly seen.

Data for LuT	Left state	Right state
α	0	1
y	0	1
z	0	1
ρ kg/m ³	725.86	43.90
u (m/s)	0	9.90
P (Pa)	$1.50 \cdot 10^7$	$8.23 \cdot 10^6$

Table 2: Initial data for an isolated rarefaction wave at equilibrium with liquid left state and vapor right state.

As an illustration, a “reference” solution can be built by introducing $\tilde{\xi}$ which corresponds to a linear regression of ξ (cf figure 18). This new quantity $\tilde{\xi}$ is continuous and monotonic; moreover, at each $\tilde{\xi}$, we can associate unique values for the quantities P , ρ , e , ϕ_2 , c . In this way, the thermodynamical path of the rarefaction wave can be projected on the (t, x) plane. Figure 19 show thermodynamical paths in the (P, T) -plane for three different meshes at the final step compared with the reference solution. Mesh refinement qualitatively improves the solution, in particular for states at low pressure. Final pressure profiles seem correct (see figure 20). Obviously, this rarefaction wave can not be used for verification purposes, the way of projecting the rarefaction wave through $\tilde{\xi}$ is not accurate

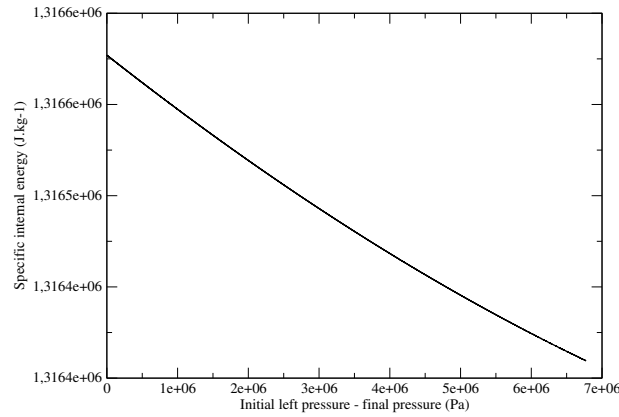


Figure 15: Specific internal energy e (in $J.kg^{-1}$) along the discrete isentropic path \mathcal{S}_{s_0} (abscissas are the opposite of the pressure gap between the final pressure and the initial left pressure equal to $150 \cdot 10^5$ Pa).

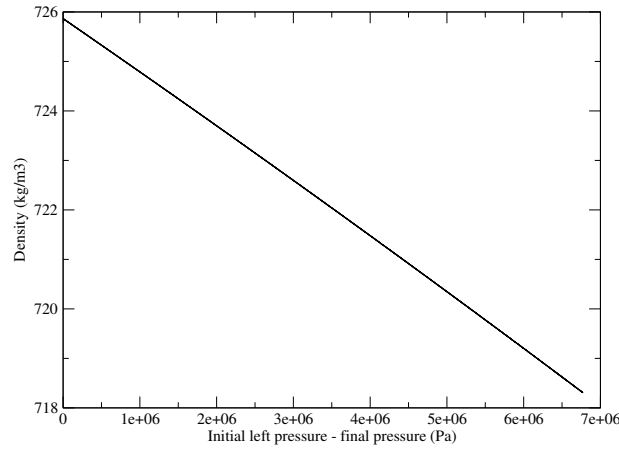


Figure 16: Density ρ (in $kg.m^{-3}$) along the discrete isentropic path (abscissas are the opposite of the pressure gap between the final pressure and the initial left pressure equal to $150 \cdot 10^5$ Pa).

enough and just allows to illustrate the encountered difficulties.

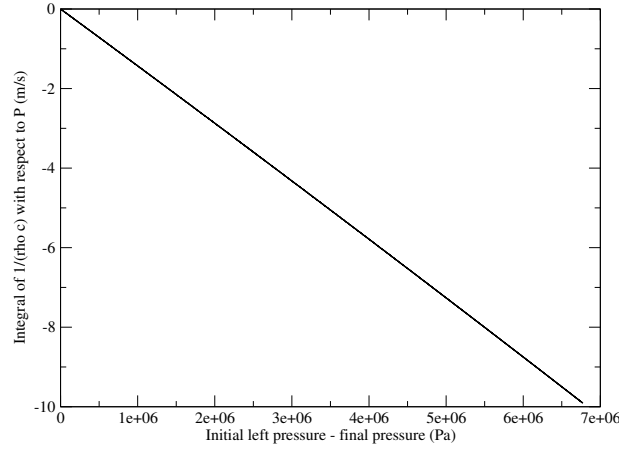


Figure 17: $\Phi_2 = \int_{P_L}^{P^*} \frac{dP}{\rho c(s_0, P)}$ (in $m.s^{-1}$) along the isentropic path (abscissas are the opposite of the pressure gap between the final pressure and the initial left pressure equal to $150 \cdot 10^5$ Pa).

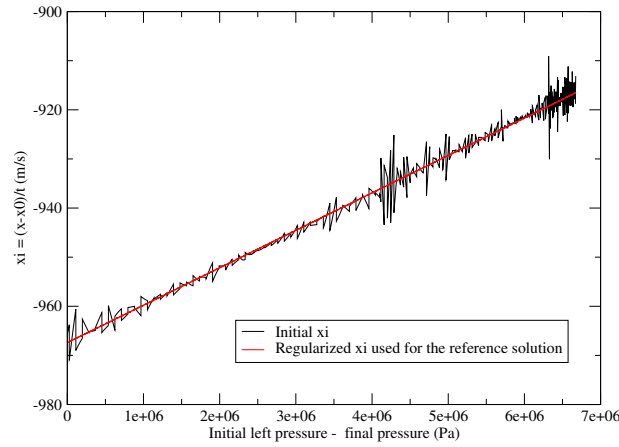


Figure 18: $\xi^* = \frac{x^* - x_0}{t} = u^* - c^*$ along the discrete isentropic path and regularized $\tilde{\xi}$ used in the reference solution (abscissas are the opposite of the pressure gap between the final pressure and the initial left pressure equal to $150 \cdot 10^5$ Pa).

C Simple model for relaxation time based on Nucleation Theory

The Classical Nucleation Theory has been developed for many years [37]. This theory assumes that the bubble nucleation rate J (the number of bubbles created per unit time in unit volume) follows an Arrhenius law:

$$J = J_0 \exp\left(-\frac{E_a}{k_B T}\right), \quad (83)$$

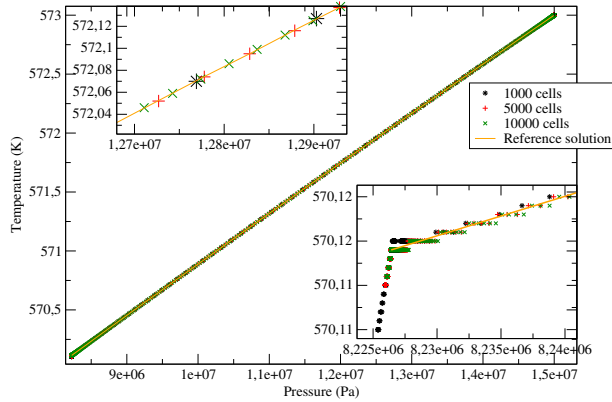


Figure 19: Thermodynamical states at the final time in the PT-plane for several meshes compared with the reference solution.

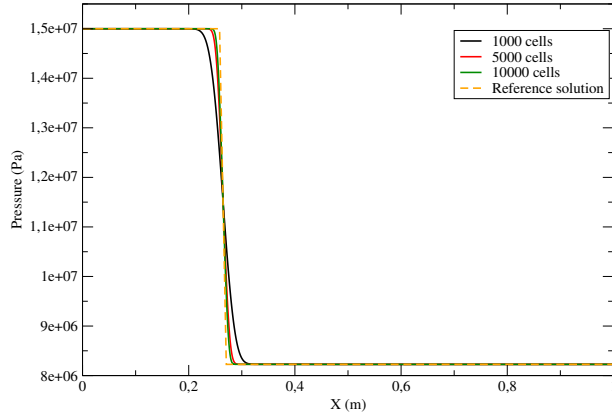


Figure 20: Pressure (Pa) as a function of X (m) at the final time compared with the reference solution.

where $k_B = 1.38064852 \cdot 10^{-23} JK^{-1}$ is the Boltzmann constant, T is the liquid temperature, J_0 is a prefactor and E_a is an activation energy. J_0 and E_a are defined in the following.

Indeed, when a bubble is created, it enables to dissipate extra energy of superheated liquid: this energy amount decreases as R^3 , with R the radius of the created bubble. At the same time, an energy amount, increasing as R^2 , is required to maintain the liquid-vapor interface. Both effects balance each other for a critical radius R_c :

$$R_c = \frac{2\gamma}{\Delta P}, \quad (84)$$

where $\Delta P = P_l - P_{sat}$ and γ is the liquid-vapor surface tension.

For spherical bubbles with a radius R_c , the required work for nucleation is minimal. This minimal nucleation work is defined as the activation energy E_a which appears in (83). It reads:

$$E_a = \frac{16\pi\gamma^3}{3(\Delta P)^2}. \quad (85)$$

It means that bubbles with a radius $R < R_c$ tend to disappear whereas bubbles with a radius $R > R_c$ are able to grow. Following an Arrhenius law (83), nucleation occurs when the barrier energy E_a has the same order of magnitude that thermal fluctuations $k_B T$. However, this energy barrier E_a can be very high because it applies to pure liquid without impurities (*homogeneous nucleation*), which are not the conditions that we may find in industrial applications. Indeed, if impurities are present in water (which is the case for nuclear circuits), bubbles creation is easier (*heterogeneous nucleation*). To take this assumption into account, the activation energy is decreased as in [1] by multiplying E_a with $\varphi \in]0, 1[$:

$$J = J_0 \exp\left(-\frac{\varphi E_a}{k_B T}\right). \quad (86)$$

Then, the probability $\mathcal{P}(t)$ that no bubble appears within a time t is:

$$\mathcal{P}(t) = \exp(-JVt)$$

where V is the volume of liquid. A common assumption [38, 39, 50] provides that nucleation indeed occurs after the time t so that: $\mathcal{P}(t) = \frac{1}{2}$. Then, a characteristic time-scale for the delay before nucleation appearance t_{nuc} can be defined with $\mathcal{P}(t_{nuc}) = \frac{1}{2}$, i.e.:

$$t_{nuc} = t_{nuc}^0 \exp\left(\frac{\varphi E_a}{k_B T}\right), \quad (87)$$

with

$$t_{nuc}^0 = \frac{\ln(2)}{J_0 V}. \quad (88)$$

There is no consensus in the litterature about the prefactor J_0 . In [51], J_0 is taken almost constant with temperature and pressure. On the contrary, complex models have been proposed, for instance in [52] or [53]. In our study, we chose a simple model, proposed in [38] or [39]. J_0 is taken as the product of thermal frequency $\frac{k_B T}{h}$ and $\frac{1}{V_c}$, where $h = 6.62607015 \cdot 10^{-34} Js$ is the Planck constant and $V_c = \frac{4\pi R_c^3}{3}$ is the volume of a critical nucleus:

$$J_0 = \frac{k_B T}{h} \frac{3}{4\pi} \frac{1}{R_c^3}. \quad (89)$$

Finally we get, with (84) and (89):

$$t_{nuc}^0 = \frac{\ln(2)}{V} \frac{1}{J_0} = \frac{\ln(2)}{V} \frac{h}{k_B T} \frac{4\pi}{3} R_c^3 = \frac{\ln(2)}{V} \frac{h}{k_B T} \frac{4\pi}{3} \left(\frac{2\gamma}{\Delta P}\right)^3.$$

We chose to simplify this prefactor: indeed, a lot of terms are almost constant during our simulations. It allows to reduce the number of parameters for our numerical studies. We keep only the dependence with $\frac{1}{\Delta P^3}$ in our final simplified model:

$$t_{nuc} = \left(\frac{a_0}{\Delta P} \right)^3 \exp \left(\frac{\varphi E_a}{k_B T} \right), \quad (90)$$

where E_a is defined by (85): $E_a = \frac{16\pi\gamma^3}{3(\Delta P)^2}$, and γ is estimated with the IAPWS 94 correlation [47]:

$$\gamma = B_0 \left(1 + b \left(1 - \frac{T}{T_c} \right) \right) \left(\frac{T}{T_c} \right)^\nu, \quad (91)$$

where: $B_0 = 235.8 \cdot 10^{-3} \text{ mN/m}$; $b = -0.625$; $\nu = 1.256$ and $T_c = 647.096 \text{ K}$ (water critical temperature).

In the simplified model (33), only two parameters have thus to be defined: a_0 in (Pa.s), homogeneous to a dynamical viscosity, and $\varphi \in [0, 1]$.

D Initial data for Riemann problems test cases

D.1 Out of equilibrium test cases (4.1)

Here are the parameters used for the Stiffened Gas (SG) for the test case of section 4.1. The parameters for the vapour are:

$$\left[\begin{array}{l} C_{V,v} = 4.477815802223535 \cdot 10^3 \text{ JK}^{-1} \text{ kg}^{-1}, \\ \gamma_v = 1.084875362318841, \\ \Pi_v = 4.1904297086743001 \cdot 10^6 \text{ Pa}, \\ s_v^0 = -1.137650328291112 \cdot 10^4 \text{ JK}^{-1} \text{ kg}^{-1}, \end{array} \right.$$

and for the liquid we have:

$$\left[\begin{array}{l} C_{V,l} = 1.395286166711847 \cdot 10^3 \text{ JK}^{-1} \text{ kg}^{-1}, \\ \gamma_l = 1.665128030303030, \\ \Pi_l = 3.725876146842836 \cdot 10^8 \text{ Pa}, \\ s_l^0 = 1.0 \cdot 10^4 \text{ JK}^{-1} \text{ kg}^{-1}. \end{array} \right.$$

Data for SG	Left state	Intermediate state
α	$4.16003754536212 \cdot 10^{-1}$	$4.68486052082106 \cdot 10^{-1}$
y	$1.0 \cdot 10^{-1}$	$1.2 \cdot 10^{-1}$
z	$1.47660058572024 \cdot 10^{-1}$	$1.75144882351565 \cdot 10^{-1}$
$\rho \text{ (kg/m}^3\text{)}$	393.940361842377	363.89814762278274
$u \text{ (m/s)}$	1.0	1.0
$P \text{ (Pa)}$	$1.48 \cdot 10^7$	$1.48 \cdot 10^7$

Data for SG	Right state
α	$4.68486052082106 \cdot 10^{-1}$
y	$1.2 \cdot 10^{-1}$
z	$1.75144882351565 \cdot 10^{-1}$
ρ (kg/m ³)	351.12092230108595
u (m/s)	-33.6320500771937
P (Pa)	$2.80621107450730 \cdot 10^6$

$\sigma = 952.696245321188e$ m/s (shock speed)

Data for LuT	Left state	Intermediate state	Right state
α	$4.16 \cdot 10^{-1}$	$4.68 \cdot 10^{-1}$	$4.68 \cdot 10^{-1}$
y	$1.0 \cdot 10^{-1}$	$1.2 \cdot 10^{-1}$	$1.2 \cdot 10^{-1}$
z	$1.48 \cdot 10^{-1}$	$1.75 \cdot 10^{-1}$	$1.75 \cdot 10^{-1}$
ρ (kg/m ³)	393.94	363.90	351.12
u (m/s)	1.0	1.0	-19.15
P (Pa)	$1.48 \cdot 10^7$	$1.48 \cdot 10^7$	$1.07 \cdot 10^7$

$\sigma = 554.61$ m/s (shock speed)

D.2 Equilibrium test case with mixtures for both initial states (4.2)

Data for LuT	Left state	Intermediate state	Right state
α	$4.16 \cdot 10^{-1}$	$6.16 \cdot 10^{-1}$	$8.31 \cdot 10^{-1}$
y	$1.0 \cdot 10^{-1}$	$2.0 \cdot 10^{-1}$	$2.84 \cdot 10^{-1}$
z	$1.48 \cdot 10^{-1}$	$2.80 \cdot 10^{-1}$	$4.20 \cdot 10^{-1}$
ρ (kg/m ³)	393.94	291.57	162.27
u (m/s)	1.0	1.0	-113.53
P (Pa)	$1.48 \cdot 10^7$	$1.48 \cdot 10^7$	$1.00 \cdot 10^7$

$\sigma = 554.607603536485$ m/s (shock speed)

D.3 Equilibrium test case with only a shock, with a liquid left initial state (4.3.1)

Data for LuT	Left state	Right state
α	0	$6.8910 \cdot 10^{-1}$
y	0	$6.73 \cdot 10^{-2}$
z	0	$1.40 \cdot 10^{-1}$
ρ (kg/m ³)	742.97	259.49
u (m/s)	1.0	-155.77
P (Pa)	$1.48 \cdot 10^7$	$5.0 \cdot 10^6$

$\sigma = 85.14$ m/s (shock speed)

D.4 Equilibrium test case with only a contact, with a liquid left initial state (4.3.2)

Data for LuT	Left state	Right state
α	0	$6.16 \cdot 10^{-1}$
y	0	$2.0 \cdot 10^{-1}$
z	0	2.8010^{-1}
ρ (kg/m ³)	742.97	291.57
u (m/s)	1.0	1.0
P (Pa)	$1.48 \cdot 10^7$	$1.48 \cdot 10^7$

References

- [1] J Bartak. A study of the rapid depressurization of hot water and the dynamics of vapour bubble generation in superheated water. *International Journal of Multiphase Flow*, 16(5):789–798, 1990.
- [2] M.R. Baer and J.W. Nunziato. A two-phase mixture theory for the deflagration-to-detonation transition (DDT) in reactive granular materials. *Journal of Multiphase Flows*, 12:861–889, 1986.
- [3] A. K. Kapila, R. Menikoff, J. B. Bdzil, S. F. Son, and D. S. Stewart. Two-phase modeling of deflagration-to-detonation transition in granular materials: Reduced equations. *Physics of Fluids*, 13(10):3002–3024, 2001.
- [4] J Glimm, D Saltz, and DH Sharp. Two-pressure two-phase flow. In *Advances In Nonlinear Partial Differential Equations And Related Areas: A Volume in Honor of Professor Xiqi Ding*, pages 124–148. World Scientific, 1998.
- [5] H Jin, J Glimm, and DH Sharp. Compressible two-pressure two-phase flow models. *Physics letters A*, 353(6):469–474, 2006.
- [6] Frédéric Coquel, Thierry Gallouët, Jean-Marc Hérard, and Nicolas Seguin. Closure laws for a two-fluid two-pressure model. *Comptes Rendus Mathématique*, 334(10):927–932, 2002.
- [7] S. Gavriluk and R. Saurel. Mathematical and numerical modeling of two-phase compressible flows with micro-inertia. *J. Comput. Phys.*, 175(1):326–360, January 2002.
- [8] G. Allaire, S. Clerc, and S. Kokh. A five-equation model for the numerical simulation of interfaces in two-phase flows. *Comptes Rendus de l’Académie des Sciences - Series I - Mathematics*, 331(12):1017 – 1022, 2000.
- [9] G. Faccanoni. *Study of a Fine Model of Liquid-Vapor Phase Change. Contribution to the Boiling Crisis Study*. PhD thesis, Ecole Polytechnique X, November 2008.

-
- [10] G. Faccanoni, S. Kokh, and G. Allaire. Modelling and simulation of liquid-vapor phase transition in compressible flows based on thermodynamical equilibrium. *Mathematical Modelling and Numerical Analysis*, 46(05):1029–1054, September 2012.
- [11] H. Guillard and A. Murrone. A five equation reduced Model for compressible two phase flow problems. Technical Report RR-4778, INRIA, March 2003.
- [12] P Downar-Zapolski, Z Bilicki, Léon Bolle, and J Franco. The non-equilibrium relaxation model for one-dimensional flashing liquid flow. *International Journal of Multiphase Flow*, 22(3):473–483, 1996.
- [13] Eric Faucher, Jean-Marc Hérard, Michel Barret, and Charles Toulemonde. Computation of flashing flows in variable cross-section ducts. *International Journal of Computational Fluid Dynamics*, 13(3):365–391, 2000.
- [14] Florence Drui. *Eulerian modeling and simulations of separated and disperse two-phase flows : development of a unified modeling approach and associated numerical methods for highly parallel computations*. PhD thesis, Université Paris-Saclay, July 2017.
- [15] Florence Drui, Adam Larat, Samuel Kokh, and Marc Massot. A hierarchy of simple hyperbolic two-fluid models for bubbly flows. *arXiv preprint arXiv:1607.08233*, 2016.
- [16] T. Barberon and P. Helluy. Finite volume simulation of cavitating flows. *Computers and Fluids*, 34(7):832–858, 2005.
- [17] Hala Ghazi. *Modélisation d’écoulements compressibles avec transition de phase et prise en compte des états métastables*. PhD thesis, Université de Nantes, 2018.
- [18] Gloria Faccanoni and Hélène Mathis. Admissible Equations of State for Immiscible and Miscible Mixtures. *ESAIM: Proceedings and Surveys*, 2019.
- [19] Stephane Jaouen. *Etude mathématique et numérique de stabilité pour des modèles hydrodynamiques avec transition de phase*. PhD thesis, Paris 6, 2001.
- [20] Philippe Helluy. *Simulation numérique des écoulements multiphasiques: de la théorie aux applications*. Habilitation à diriger des recherches, Université du Sud Toulon Var, 2005.
- [21] H. Mathis. *Theoretical and numerical study of phase transition flows*. PhD thesis, Université de Strasbourg, September 2010.
- [22] J. Jung. *Numerical simulations of two-fluid flow on multicores accelerator*. PhD thesis, Université de Strasbourg, October 2013.
- [23] P. Helluy and N. Seguin. Relaxation models of phase transition flows. *ESAIM: Mathematical Modelling and Numerical Analysis*, 40(2):331–352, 2006.

-
- [24] O. Hurisse. Application of an homogeneous model to simulate the heating of two-phase flows. *International Journal on Finite Volumes*, 11:<http://www.latp.univ-mrs.fr/IJFV/spip.php?article52>, May 2014.
- [25] Olivier Hurisse. Numerical simulations of steady and unsteady two-phase flows using a homogeneous model. *Computers and Fluids*, 152, July 2017.
- [26] P. Helluy, O. Hurisse, and E. Le Coupanec. Verification of a two-phase flow code based on an homogeneous model. *International Journal on Finite Volumes*, 13, November 2016.
- [27] O Métayer, Jacques Massoni, and Richard Saurel. élaboration des lois d'état d'un liquide et de sa vapeur pour les modèles d'écoulements diphasiques. 43:265–276, 03 2004.
- [28] Malte Hoffmann. *An Explicit Discontinuous Galerkin Method for Parallel Compressible Two-Phase Flow*. PhD thesis, University of Stuttgart, 2017.
- [29] W. Wagner and H.-J. Kretzschmar. *International Steam Tables: Properties of Water and Steam Based on the Industrial Formulation IAPWS-IF97*. Springer-Verlag Berlin Heidelberg, 2008.
- [30] Viktor Vladimirovich Rusanov. The calculation of the interaction of non-stationary shock waves with barriers. *Zhurnal Vychislitel'noi Matematiki i Matematicheskoi Fiziki*, 1(2):267–279, 1961.
- [31] T. Buffard, T. Gallouët, and J.-M. Hérard. A sequel to a rough Godunov scheme: application to real gases. *Computers and Fluids*, 29(7):813–847, 2000.
- [32] C. Chalons and J.-F. Coulombel. Relaxation approximation of the euler equations. *Journal of Mathematical Analysis and Applications*, 348(2):872 – 893, 2008.
- [33] I Suliciu. On the thermodynamics of fluids with relaxation and phase transitions. fluids with relaxation. *Internat. J. Engrg. Sci*, 36:921–947, 1998.
- [34] Frédéric Coquel and Benoît Perthame. Relaxation of energy and approximate riemann solvers for general pressure laws in fluid dynamics. *SIAM Journal on Numerical Analysis*, 35(6):2223–2249, 1998.
- [35] François Bouchut. *Nonlinear stability of finite Volume Methods for hyperbolic conservation laws And Well-Balanced schemes for sources*. Springer Science & Business Media, 2004.
- [36] Frédéric Coquel, Edwige Godlewski, and Nicolas Seguin. Relaxation of fluid systems. *Mathematical Models and Methods in Applied Sciences*, 22(08):1250014, 2012.
- [37] Pablo G Debenedetti. *Metastable liquids: concepts and principles*. Princeton University Press, 1996.

-
- [38] Frédéric Caupin and Eric Herbert. Cavitation in water: a review. *Comptes Rendus Physique*, 7(9-10):1000–1017, 2006.
- [39] Humphrey J Maris. Introduction to the physics of nucleation. *Comptes Rendus Physique*, 7(9-10):946–958, 2006.
- [40] B. Riegel. *Contribution à l'étude de la décompression d'une capacité en régime diphasique*. PhD thesis, 1978.
- [41] Olivier Hurisse and Lucie Quibel. A homogeneous model for compressible three-phase flows involving heat and mass transfer. *ESAIM: Proceedings and Surveys*, 2019.
- [42] N.N. Yanenko. *Méthode à pas fractionnaires: résolutions de problèmes polydimensionnels de physique mathématique*. Collection Intersciences. A. Colin, 1968.
- [43] Shi Jin and Zhouping Xin. The relaxation schemes for systems of conservation laws in arbitrary space dimensions. *Communications on pure and applied mathematics*, 48(3):235–276, 1995.
- [44] Christophe Chalons and Frédéric Coquel. Navier-stokes equations with several independent pressure laws and explicit predictor-corrector schemes. *Numerische Mathematik*, 101(3):451–478, 2005.
- [45] E.F. Toro. *Riemann Solvers and Numerical Methods for Fluid Dynamics: A Practical Introduction*. Springer Berlin Heidelberg, 2009.
- [46] T. Gallouët, J.-M. Hérard, and N. Seguin. Some recent Finite Volume schemes to compute Euler equations using real gas EOS. *International Journal for Numerical Methods in Fluids*, 39:1073–1138, 2002.
- [47] T Petrova and RB Dooley. Revised release on surface tension of ordinary water substance. *Proceedings of the International Association for the Properties of Water and Steam, Moscow, Russia*, pages 23–27, 2014.
- [48] H. B. Callen. *Thermodynamics and an Introduction to Thermostatistics*. John Wiley & sons, 1985.
- [49] H. Mathis. A thermodynamically consistent model of a liquid-vapor fluid with a gas. *ESAIM: M2AN*, 53(1):63–84, 2019.
- [50] Mouna El Mekki, Claire Ramboz, Laurent Perdereau, Kirill Shmulovich, and Lionel Mercury. Lifetime of superheated water in a micrometric synthetic fluid inclusion. In *Metastable Systems under Pressure*, pages 279–292. Springer, 2010.
- [51] GV Ermakov and EV Lipnyagov. Criterion of homogeneous boiling-up of superheated liquids. *Thermophysics and Aeromechanics*, 15(4):623–630, 2008.

-
- [52] D Turnbull and J Co Fisher. Rate of nucleation in condensed systems. *The Journal of chemical physics*, 17(1):71–73, 1949.
- [53] Emmanuel Clouet. Modeling of nucleation processes. *arXiv preprint arXiv:1001.4131*, 2010.